EVALUATION OF PILOT'S ABILITY TO STABILIZE A FLEXIBLE LAUNCH VEHICLE DURING FIRST-STAGE BOOST

By Gordon H. Hardy,* James V. West,** Robert W. Gunderson,*** and Charles O. Jones***

*Research Scientist and Pilot, NASA-Ames Research Center, Moffett Field, California

**Research Scientist, NASA-Ames Research Center, Moffett Field, California

***Research Scientist, NASA-Marshall Space Flight Center, Hunstville Alabama

AIAA Astrodynamics Guidance & Control Conference, U. of Calif., Aug. 24-26, 1964

EVALUATION OF PILOT'S ABILITY TO STABILIZE A FLEXIBLE LAUNCH VEHICLE DURING FIRST-STAGE BOOST

By Gordon H. Hardy,* James V. West,** Robert W. Gunderson,*** and Charles O. Jones***

SUMMARY

A preliminary manual control system for the S-IC, or first, stage of the Saturn V launch vehicle was designed and evaluated. With the exception of fuel sloshing dynamics (for which the data were not available), a complete fixed-base simulation was used. The results indicate that satisfactory manual control is possible.

INTRODUCTION

There has been considerable speculation that pilot participation in guidance and control of large launch vehicles could conceivably increase the probability of successful mission accomplishment. Some study of this question has already been completed, most notably for the Titan III[1-4] and the somewhat earlier investigation by Holleman and Armstrong.[5] These and other studies have shown that, generally speaking, the guidance and control of large booster systems is sufficiently within piloted system capabilities

---

*Research Scientist and Pilot, NASA-Ames Research Center, Moffett Field, California

**Research Scientist, NASA-Ames Research Center, Moffett Field, California

***Research Scientist, NASA-Marshall Space Flight Center, Huntsville, Alabama

as to warrant serious consideration. Other than by such general statements, however, the question of pilot participation should be discussed only within the reference formed by particular vehicle configurations and flight profiles. The Marshall Space Flight Center and Ames Research Center are currently engaged in a joint research study intended to determine pilot capabilities and the feasibility of utilizing any such capabilities to obtain an increase in over-all reliability of the Saturn V launch vehicle. In particular, the completed study will have investigated the ability of a piloted system to accomplish attitude stabilization, structural load reduction, and guidance functions for the entire Saturn V flight profile.

The purpose of this report is to present results obtained on investigation of the first (S-IC) stage of the flight profile. During this part of the study the assumption is made that the guidance function is accomplished through conventional, automatic system, implementation. Consequently, the piloted system capability question reduces essentially to an investigation of the control tasks arising from attitude stabilization and structural load reduction requirements. In addition to the attitude stabilization and load reduction responsibilities, the pilot was required to accomplish a roll maneuver at lift-off and accomplish a pitch plane tilt program. The initial simulation was carried out on a fixed time of flight, rigid body dynamics, two-degree-of-freedom simulation. The complexity was gradually increased to the final form consisting of rigid body, plus flexible body dynamics, five

degrees of freedom, and continuous time of flight from lift-off to the completion of the first stage. Fuel sloshing dynamics were not considered and will be examined when the data becomes available. It should be emphasized that the control system configuration, pilot responsibilities, and piloting techniques discussed in this report are not necessarily those which will be recommended in the final analysis.

NOTATION

c.g.	center of gravity
$F_\alpha, F_\varphi, F_\beta, M_\alpha, M_\beta, M_\beta', K_{i_1}, K_{i_2}$	time varying coefficients
g	sea level value of earth's acceleration
l_a	distance from vehicle c.g. to accelerometer measured positive forward, meters
$\frac{M_x}{M_D}$	rigid body bending moment at station x, normalized to design value
S	Laplace operator
V	nominal vehicle velocity, meters per second
X_i	vehicle c.g. location with respect to nominal location, meters
α_i	aerodynamic angle of attack, deg
α_{w_i}	component of angle of attack due to wind, deg
β_i	engine gimbal angle, deg

$\ddot{\gamma}_i$ accelerometer output, meters per second per second

η_i generalized elastic bending mode amplitude

ω_n natural frequency, radians/sec

φ_i total attitude angle with respect to a space fixed coordinate system, deg

$\Delta\varphi_i$ attitude error sensed by the inertial navigator, deg

$\Delta\varphi_i^*$ rigid body attitude error, deg

χ_i nominal vehicle attitude with respect to a space fixed coordinate system, deg

ζ damping ratio

Subscripts

P pitch

Y yaw

R roll

DESCRIPTION OF SIMULATION

Vehicle Description

The example vehicle used in this study was the Saturn V launch vehicle as defined for the Apollo lunar landing mission. As shown in Fig. 1, the vehicle configuration consists of three booster stages and the Apollo spacecraft. Over-all vehicle length is 364 feet and the maximum diameter is 396 inches (not including fins). Fully fueled weight is approximately 6,000,000 pounds.

The launch vehicle is powered by three liquid fueled stages. Five F-1 engines with a total nominal thrust of 7,500,000 pounds power the first stage (designated S-IC). The second stage (designated S-II) is powered by five J-2 engines with a total nominal thrust of 1,000,000 pounds. One J-2 engine with restart capability and a nominal thrust of 200,000 pounds power the third stage (designated S-IVB).

The Saturn V launch vehicle has an inertial navigation and guidance system independent of the one contained in the Apollo spacecraft. A control system computer and necessary sensors are also located in the launch vehicle.

Detailed vehicle characteristics may be found in reference 6.

Trajectory Description

The primary mission of the Saturn V launch vehicle is to inject the Apollo spacecraft, which weighs approximately 90,000 pounds, into a translunar trajectory. This is accomplished by inserting the S-IVB stage and Apollo spacecraft into a 100 nautical mile earth orbit which requires a partial burn of the S-IVB propellants. A second burn of the S-IVB engine then injects the S-IVB stage and Apollo spacecraft into a translunar trajectory from the earth orbit.

However, for the present report, we are concerned with the trajectory from launch through first stage (S-IC) burnout. This stage burns for 150 seconds and stages at approximately 60,000 meters altitude and at a velocity of 2,350 meters per second. The maximum thrust-to-weight ratio is 4.7 while the maximum dynamic pressure (3,650 kilograms per square meter) occurs at an altitude of about 13,000 meters.

Detailed trajectory data are contained in reference 6.

Wind Environment

The primary trajectory disturbance during first stage of flight is the wind environment. The wind environment used in this study is specified in the Saturn V launch vehicle design data document, reference 6. These wind profiles are based on statistical analysis of wind measurements taken at the Atlantic Missile Range, Cape Kennedy Launch Area. Values of steady-state wind, wind shear, gusts, and turbulence are given. Steady-state winds are always assumed horizontal with no restriction on direction. For any particular system, the combination of steady-state wind, wind shear, gusts, and turbulence which provides the greatest excitation should be used.

Figure 2 presents the wind used for this report. The maximum wind speed is 75 meters per second while the maximum value of wind shear occurs near the point of maximum dynamic pressure.

Vehicle Design Constraints

The principal constraints placed on the design of the launch guidance and control system are guidance accuracy and structural loads. Since the study of the present report only considers the first stage of flight the structural loads were the primary constraint. This follows conventional design philosophy of letting the structural loads take precedence during the early stages of flight and guidance take precedence during the final stages.

Performance measures were specified and are intended to show how well the system has satisfied the design constraints. The

performance measures used in this study are described in the following paragraphs.

The primary performance measure used was the rigid body bending moment occurring at the critical location on the vehicle. This bending moment was calculated with the expression

$$M_x = \frac{\partial M_x}{\partial \alpha} \alpha + \frac{\partial M_x}{\partial \beta} \beta$$

where

M_x rigid body bending moment at station x

$\frac{\partial M_x}{\partial \alpha}$ function of mass distribution and aerodynamic loading, constant at a given time of flight at station x

$\frac{\partial M_x}{\partial \beta}$ function of mass distribution and thrust, constant for a given time of flight at station x

The resultant of the pitch and yaw moments, normalized to unity at the limit design bending moment, is used for data presentation.

Flexible body dynamics also contribute to structural loading, but data necessary for computation of the moment due to bending mode acceleration terms were not available at the time of the simulation. Consequently, a design goal of minimization of the bending acceleration terms was imposed. This is also important to reduce objectionable motion cues sensed by the pilot. The amplitudes of the generalized bending acceleration terms, $\ddot{\eta}_i$, furnished the performance measure. Data are presented in terms of the flexible body accelerations felt by the pilot.

A measure of how well the pilot could control to the nominal trajectory was obtained by measuring the distance and velocity dispersions normal to nominal trajectory at the first-stage cutoff point. As

mentioned previously, however, trajectory control during first stage of the boost profile is considered a less stringent constraint than structural loading.

The final performance measure used was the numerical Cooper Pilot Opinion Rating System shown in Fig. 3. This rating is the pilot's subjective opinion of how well he was able to control the system with respect to the task assigned. Reference 7 describes the Cooper Rating System in detail.

Control System Description

Attitude control of the Saturn V during the powered flight of the S-IC stage is accomplished by swiveling the four outboard F-1 engines. The maximum allowable deflection is five degrees for each engine in any direction. The center engine does not swivel.

The roll control system developed during the study was a simple rate system.

Figure 4 shows the configuration of the pitch and yaw manual control systems. It will be noted that the augmentation system consists of a single (rate) loop. Attitude, attitude error, attitude rate, and accelerometer signals from body mounted normal accelerometers are displayed to the pilot.

The basic configuration, or loop structure, was determined by rigid body studies. Introduction of elastic body dynamics dictated the addition of two filters (rate augmentation filter and controller output filter) in order to maintain system stability.

The rigid body vehicle is inherently unstable because of the aft location of the c.g. This instability varies with time of flight and reaches a peak value (ω_n^2 about -.15) near the time of flight corresponding to maximum dynamic pressure. The lowest flexible body mode frequency is just over one cycle per second.

The engine dynamics were approximated by the following transfer function

$$\frac{\beta(S)}{\beta_c(S)} = \frac{27{,}000}{(S + 30)(S^2 + 18S + 900)}$$

In addition, the engine was rate limited.

The fixed cockpit used is shown in Fig. 5 while Fig. 6 shows instrument panel details. The two large instruments are standard aircraft all-attitude indicators, with the upper one being used as the primary flight instrument. The upper indicator is rotated clockwise 90° from the standard aircraft orientation to simulate the Apollo all-attitude indicator gimbal order. Vehicle attitude is displayed on the sphere of this indicator with pitch and yaw attitude errors being presented on the flight director needles. Scaling on these needles was 10° attitude error per inch. Body mounted normal accelerometer outputs are displayed on the flight director needles of the lower all-attitude indicator and are scaled ±1/8 g per inch. The sphere of this second instrument was not used. Vehicle attitude rates are presented on the d.c. meters at the upper center and upper right of the display panel. Deflection of a 45° meter corresponded to a 4° per second attitude rate. A standard aircraft, elapsed-time clock is mounted to the left of the primary all-attitude indicator.

Figures 7 and 8 show the two-axis side-arm "pencil" controller and rudder pedals used early in the study. The three-axis side-arm controller used for the later phases of the study is shown in Fig. 9. All the controllers had outputs that were nearly linear with displacement.

Simulation Equations

The rigid body equations of motion simulated were a perturbation set with respect to a reference frame moving along the nominal trajectory.

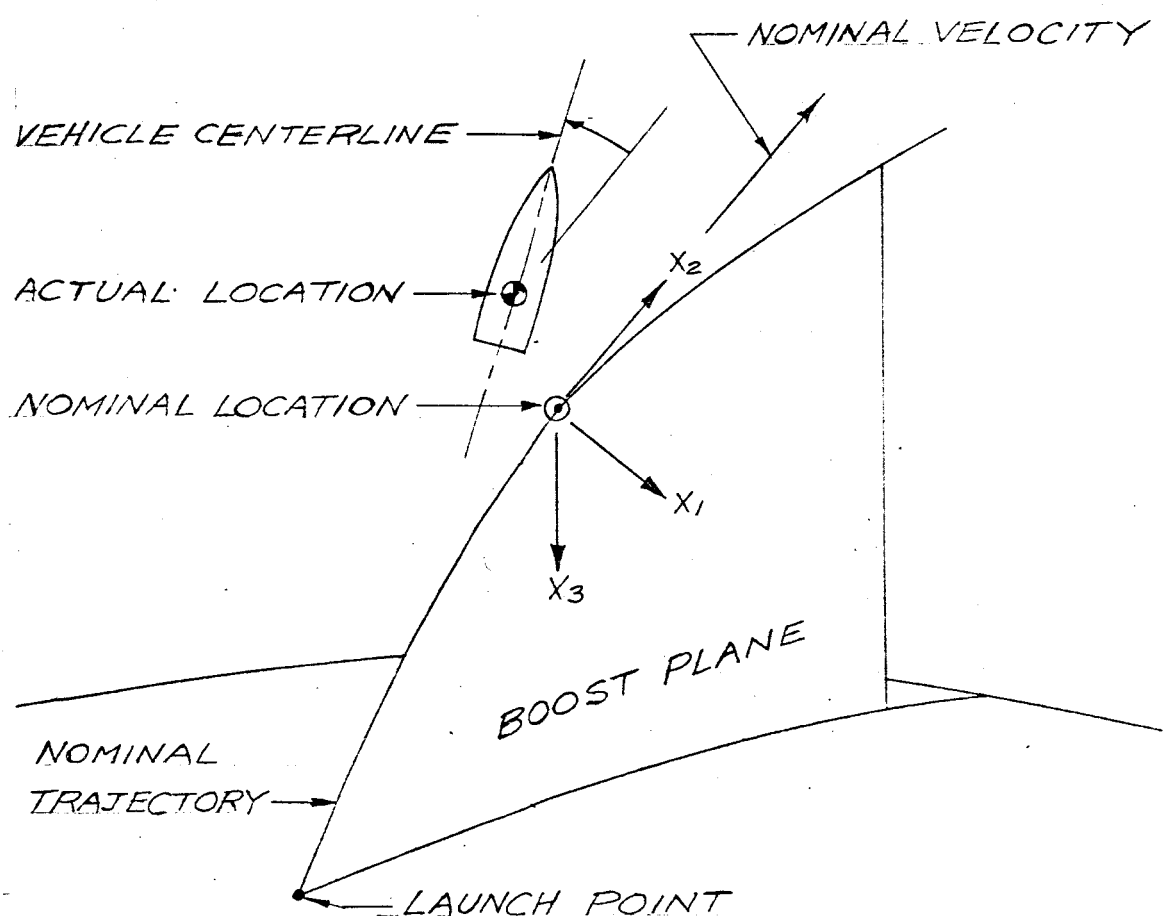

Axes x_1, x_2, x_3 form a right-hand orthogonal system with x_2 alined along the nominal velocity vector and axes x_1, x_2 lying in the nominal boost plane. While fuel sloshing modes were not analyzed, up to two structural elastic modes were included. The linearized, time varying coefficient equations including the ith elastic mode are given below.

Rigid body:

(1) $$\ddot{x}_1 = -F_\alpha \alpha_P - F_\varphi \Delta\varphi_P - F_\beta \beta_P$$

(2) $$\ddot{x}_3 = F_\alpha \alpha_Y + F_\varphi \Delta\varphi_Y + F_\beta \beta_Y$$

(3) $$\Delta\ddot{\varphi}_Y^* = M_\alpha \alpha_Y - M_\beta \beta_Y$$

(4) $$\Delta\ddot{\varphi}_R^* = -M_\beta' \beta_R - \ddot{x}_Y$$

(5) $$\Delta\ddot{\varphi}_P^* = M_\alpha \alpha_P - M_\beta \beta_P$$

(6) $$\ddot{\gamma}_1 = -F_\alpha \alpha_P - F_\beta \beta_P - \frac{l_a}{57.3} \Delta\ddot{\varphi}_P^*$$

(7) $$\ddot{\gamma}_3 = -F_\alpha \alpha_Y + F_\beta \beta_Y + \frac{l_a}{57.3} \Delta\ddot{\varphi}_Y^*$$

(8) $$\alpha_Y = \Delta\varphi_Y^* + \alpha_{W_P} - \frac{57.3}{V} \dot{x}_3$$

(9) $$\alpha_P = \Delta\varphi_P^* + \alpha_{W_P} + \frac{57.3}{V} \dot{x}_1$$

Elastic body (ith mode)

(1) $$\ddot{\eta}_{i_Y} + 2\zeta\omega\dot{\eta}_{i_Y} + \omega^2\eta_{i_Y} = K_{i_1}\beta_Y + K_{i_2}\ddot{\beta}_Y$$

(2) $$\ddot{\eta}_{i_P} + 2\zeta\omega\dot{\eta}_{i_P} + \omega^2\eta_{i_P} = K_{i_1}\beta_P + K_{i_2}\ddot{\beta}_P$$

Total perturbations (attitude angles only)

(1) $$\Delta\varphi_Y = \Delta\varphi_Y{}^* + K_3\eta_Y$$

(2) $$\Delta\varphi_R = \Delta\varphi_R{}^*$$

(3) $$\Delta\varphi_P = \Delta\varphi_P{}^* + K_3\eta_P$$

Total attitude angles (for pilot display only)

(1) $$\varphi_Y = \Delta\varphi_Y$$

(2) $$\varphi_R = \Delta\varphi_R + \chi_R$$

(3) $$\varphi_P = \Delta\varphi_P + \chi_P$$

where χ_R and χ_P are the nominal values of roll and pitch, respectively.

The symmetric configuration of Saturn V permitted inertia product and aerodynamic coupling to be neglected. Nonlinear terms in the equations of motion were considered but found to have negligible effect for the ranges of perturbations considered.

RESULTS AND DISCUSSION

Design Method

The design approach used for the preliminary manual control system consisted of three major phases as follows:

Basic handling qualities.- The objective of this portion of the study was to determine the basic control system configuration. In this phase the type of stability augmentation, rigid body gain coefficients, and parameters for pilot display were determined. A five-degree-of-freedom rigid body, three axis, discrete time of flight simulation was used.

Filter design.- In this phase of the study, the design of the filters as dictated by the elastic body dynamics was accomplished. This included the rate loop augmentation filter, the pilot's controller filter, and an investigation of display filters. A single axis, two-degree-of-freedom rigid body plus flexible body, discrete time of flight simulation was used.

Primary manual performance.- From the basic handling qualities and filter design phases of study a piloted control system was developed. The object of this last phase of study was to test this system on a more realistic simulation and measure system performance. A realistic three axis, five-degree-of-freedom rigid body plus elastic body, continuous time of flight simulation was used. Emphasis was placed on developing pilot techniques to produce the desired performance.

Basic Handling Qualities

Simulation.- The discrete time of flight chosen was that corresponding to maximum dynamic pressure. Since the maximum steady-state wind and maximum wind shear both occur near this time of flight, it was felt, and later justified, that this would be the critical design point of the trajectory. The wind disturbance used was similar to that shown in Fig. 2 but was idealized to a ramp input building from 0 to 75 meters per second at a rate of 10 meters per second per second. A random noise generator

supplied a turbulence condition which was superimposed on the basic wind profile. Maximum amplitude of the turbulence was approximately 7.5 meters per second, measured peak to peak. The wind was randomly rotated in direction between each piloted run. The runs were approximately 30 seconds to 1 minute in duration with the ramp wind disturbance commencing some random time after run initiation.

Initial results were obtained with the two-axis side-arm controller and rudder pedals while the three-axis controller was used later. The particular controller used is indicated on the results. The three-axis controller was more representative of Apollo hardware and was used as soon as it became available. Performance comparisons showed little relative advantage for either controller.

Pilot task.- The pilot task for this phase of the study was to minimize the rigid body bending moment, while stabilizing the roll attitude, in the presence of the wind disturbance. This task is more difficult than attitude stabilization alone as it requires maneuvering the vehicle through several degrees of attitude change. As discussed in the design constraints section, aerodynamic angle of attack and engine gimbal angle both contribute to the rigid body bending moment. The pilot attempted to zero the angle of attack by utilizing the body mounted accelerometer signals displayed on the flight director needles, while minimizing engine gimbal angles by making the minimum required controller inputs. Experience indicated the proper magnitude of controller input necessary.

Results and discussion.- Previous experience, see reference 5, indicated that with the relatively small static instability present the rigid body vehicle could be controlled with rate augmentation only. For this case, assuming satisfactory displays and controller, there are only two gains per channel to choose in the control system design. These are the rate loop gain coefficient and the pilot's controller sensitivity. Figures 10 and 11 present pilot rating and maximum rigid body bending moment, respectively, as a function of these two parameters. The abscissas are controller sensitivity presented as the maximum engine deflection angle obtainable with full controller deflection. The ordinates are the rate loop gain coefficient and are proportional to the system damping, $2\zeta\omega_n$. The parameter values were varied simultaneously in the pitch and yaw channel. The rate loop gain coefficient in the roll channel was set to correspond to a time constant of 0.9 second while the roll channel controller sensitivity was fixed at about 15° per second^2.

The significant result shown is the insensitivity of performance to the two parameters. Design values of 0.75 for rate gain coefficient and 3.0 for controller sensitivity were chosen. This value of damping would give a time constant of about 1.2 seconds for neutral stability. Because of the dependence of rigid body bending moment on engine gimbal angle, the best bending moment performance occurred at controller sensitivities slightly lower than that for best pilot rating. At still lower controller sensitivities the vehicle becomes uncontrollable due to the inability to command sufficient engine angle. At higher values the controller is overly sensitive. Although the figures indicate that control is possible

for no rate augmentation, it must be recalled that the simulation was highly idealized.

The body mounted accelerometers were mounted at the vehicles instantaneous center of rotation for the data runs presented in Figs. 10 and 11. This location is about 15 meters forward of the vehicles center of gravity (c.g.) at maximum dynamic pressure. At this location, the accelerometer signal due to vehicle rotation resulting from an engine deflection is exactly cancelled by the acceleration signal due to vehicle translation. This may be seen by combining rigid body Eqs. (5) and (6) to give the accelerometer signal in terms of angle of attack and gimbal angle.

$$\ddot{\gamma} = -\left(F_\alpha + \frac{l_a}{57.3} M_\alpha^{\cdot}\right)\alpha - \left(F_\beta - \frac{l_a}{57.3} M_\beta\right)\beta$$

For the instantaneous center of rotation (no β contribution) the accelerometer location, l_a, is:

$$l_a = 57.3 \frac{F_\beta}{M_\beta}$$

The remaining signal is then proportional to α. Figure 12 shows the effect in pilot opinion and bending moment of moving the accelerometer from this location. The abscissa represents longitudinal location of the accelerometer forward of the c.g., made dimensionless to the distance to the instantaneous center of rotation. In the first equation above, changing l_a will cuase the coefficient of the β term to be either positive or negative. By moving the accelerometer aft, vehicle translation acceleration predominates which causes a very confusing

signal for pilot control. Consequently, the performance as shown in Fig. 12 deteriorates rapidly. Moving the accelerometer forward causes the rotational component of the signal to predominate which provides a signal which tends to reduce angular accelerations and is not nearly as confusing to the pilot. The figure shows that the performance is relatively insensitive to accelerometer location over a range of about 15 meters and then deteriorates slowly. The design point for the remainder of the study was arbitrarily chosen as the instantaneous center of rotation at maximum dynamic pressure.

To validate the assumption that a rate augmentation only system would not cause large decrements in performance compared with more complex augmentation, an accelerometer loop was added to the control system of Fig. 4. Figure 13 shows bending moment performance and pilot rating as a function of the accelerometer loop gain coefficient. Positive values increased the stability and the value for neutral stability is noted. Increasing the stability had little effect on bending moment performance; but since the pilot's task of nulling the accelerometer is eased, the pilot rating improves. As an indication of the control system sensitivity to vehicle stability level, values of accelerometer gain corresponding to decreased stability margins were also investigated. Bending moment performance deteriorated slowly indicating insensitivity to a value where the pilot became saturated and the vehicle became uncontrollable.

Bending Filter Design

Rate augmentation filter.- The rate augmentation filter is required to stabilize the elastic structural dynamics present in the closed rate loop. With respect to the Saturn V vehicle, this problem is complicated by the relatively narrow separation of the first bending mode natural frequency from the rigid body control frequencies. The design of this filter for a manual attitude control system is, in principal, no different from that normally used for automatic control systems. The procedure involves finding a filter which attenuates or shifts the phase of the bending content of the feedback signals such that adequate stability margins are attained but which does not "significantly" alter the rigid body content of the signals.

A satisfactory rate augmentation filter for the manual control system was determined to be

$$F_1(S) = \frac{336}{(S + 6)(S + 7)(S + 8)}$$

Any response modes introduced by this filter were heavily damped and not objectionable to the pilot.

Controller filter.- The purpose of this filter is to smooth the output of the pilot's controller at elastic bending frequencies. In conjunction with the augmentation filter described previously, this reduces the magnitude of the structural oscillations or "springboard" effect. This is important for three considerations:

(1) The rigid body control task is not obscured at the pilot's displays by elastic oscillations. (Another approach to this problem would smooth the sensor outputs.)

(2) The component of bending moment stress due to elastic structural motions is reduced.

(3) Motions at the pilot's station due to elastic motions are reduced. This may be necessary if the motions are severe enough to complicate the pilot's control task.

As seen in Fig. 4, the phase lags introduced by the controller and any display filters will be additive. Therefore, the introduction of display filters will affect the controller filter design. Based on consideration (1) alone, it is not clear what combination of controller and display filters should be used. Considerations (2) and (3) though, both require the introduction of as much phase lag as is allowable at the controller filter. The best over-all solution then is to place the total allowable phase lag, from rigid body control considerations, in the controller filter.

For the present preliminary manual control system, a passive second-order filter configuration was chosen.

$$F_2(S) = \frac{\omega_n^2}{S^2 + 2\zeta\omega_n S + \omega_n^2}$$

Piloted simulation runs were made varying the natural frequency ω_n of this filter, with a fixed damping ratio, ζ, of 0.5 to produce the results shown in Fig. 14. A fixed time of flight, two-degree-of-freedom rigid body plus flexible body, single axis simulation was used. Other characteristics of the simulation and the pilot task were identical to that used for the basic handling qualities investigation described previously.

The upper curves of Fig. 14 show pilot rating and rigid body bending moment performance while the lower curve presents the maximum amplitude

of the structural elastic motions at the pilot's station for the first and second modes. Lowering the natural frequency of the filter attenuates the pilot's inputs which occur at body elastic frequencies but the phase lag introduced causes the rigid body control problem to become more difficult with a corresponding increase in the maximum bending moment. Based on preliminary data on the relative significance of the rigid body bending moment and elastic motions, the design value indicated was chosen for the remainder of the study.

To test the sensitivity of the control system to variations in the first elastic mode frequency the results shown in Fig. 15 were obtained. As expected, a lowering of the natural frequency causes a decrement in the three performance criteria. The figure indicates, that for the expected frequency variation of less than 20 percent, the design is satisfactory.

Figures 16 and 17 indicate that from a piloted standpoint, only the first bending mode is significant as the elastic motion amplitudes for this mode are much larger than for the second mode. Therefore, it will be the dominant elastic effect seen at the pilot's displays and in his motion cues. In later piloted simulations only the first mode was mechanized. It should be recalled, however, that all the structural modes must be included in the design of the rate augmentation filter.

Manual Performance

Saturn V first stage manual control performance was obtained during this phase of the study. A complete simulation was used and different piloting techniques evaluated.

Simulation.- The controller used was the three-axis side-arm controller shown in Fig. 9. The wind disturbance used in this phase of study was discussed in Fig. 2 and was randomly rotated in direction for each piloted computer run. The pitch and yaw channel control system is shown in Fig. 4 while the roll channel was a simple rate system with a time constant of 1.9 seconds.

Simulation runs commenced at lift-off with run duration corresponding to the time of flight for the first stage. Strip recordings were made of significant parameters and a typical run is shown in Fig. 16.

Pilot tasks.- Several pilot tasks were evaluated to determine how they affected system performance. Each task emphasized some particular performance criteria while compromising on others. The tasks were divided into two groups, a primary task (attitude stabilization or load control) being associated with each group. Within each group secondary tasks were assigned. This breakdown of tasks is tabulated along the abscissas of Figs. 17 through 24.

Attitude stabilization: For task numbers 1 through 4 the primary task assigned was attitude stabilization or nulling the attitude error signals in pitch and yaw while maintaining the correct roll angle. The roll angle program called for a 40° roll after lift-off to the desired heading and zero roll angle therafter. About five seconds prior to staging, the pilot let the rate augmentation system take over and null the attitude rates for staging.

For task number 1, no secondary task was assigned.

For task numbers 2 and 3, the secondary task was control of trajectory dispersions. These were assumed to be the distances normal to the nominal

trajectory at any given time in the pitch and yaw planes. For task number 2, in addition to attitude stabilization, the pilot used the signals from the body mounted accelerometers to minimize trajectory dispersions in a manner similar to "drift minimum control" for an automatic system.

For task number 3, the dispersions normal to the nominal trajectory were displayed to the pilot to allow direct control to the nominal trajectory. Emphasis was not placed on this task since trajectory guidance is beyond the scope of this report.

For task number 4, the rate augmentation loop was opened and the pilot was required to supply rate augmentation by the use of displayed attitude rates. With the present preliminary control system, three-axis control without rate augmentation is marginal. Therefore, only single-axis data is shown. The pitch and roll channels were controlled by an automatic system and the pilot controlled the yaw channel.

Load reduction: For task numbers 5 through 7, the primary task assigned was "load" reduction. As discussed in the section on vehicle constraints, the vehicle structural load or bending moment is a combination of aerodynamic loads and engine induced loads. Since the aerodynamic loads are only significant in the high dynamic pressure region, the recommended piloting procedure utilized the signals from the body mounted accelerometers during this period.

For task number 5, the pilot was required to stabilize the pitch and yaw attitude error signals from lift-off to 60 seconds. At 60 seconds through 90 seconds he placed primary emphasis on nulling the accelerometer

signals while maintaining zero roll angle. Figure 2 indicates that this is the period during which extreme winds can be expected. From 90 seconds to 105 seconds, he gradually returns to the attitude error signals while maintaining the accelerometer signals at a safe level. After 105 seconds, the procedure is identical to the attitude stabilization task. Throughout the flight the pilot minimizes the engine induced loads by making smooth, small controller inputs.

Task number 6 is identical to 5 except in the way the pilot detects attitude error signals. The upper flight director needles were deactivated and the nominal pitch attitude program was placed on a scale around the pilot's clock as shown below. By reading the correct value

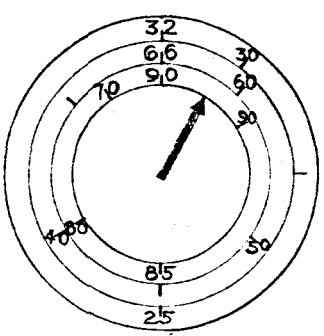

of pitch attitude as a function of time and comparing with the actual value on the all-attitude indicator, the pilot could obtain the pitch attitude error. Since the yaw attitude should be constant during first-stage boost, the pilot controls yaw and roll attitude directly from the all-attitude indicator.

Task number 7 is similar to 4 in that the pilot must supply the rate augmentation.

Results and discussion.- Figures 17 through 24 present significant trajectory performance parameters for the seven pilot tasks chosen. Five pilots participated in the study and each flew at least three trajectories for each of the tasks. At the end of each task the pilot was asked for a pilot rating for the task. Performance data for an automatic system which had attitude and attitude rate feedback is also indicated for reference.

Figure 17 presents the Cooper Scale Pilot Rating for each task. As expected, the more complex tasks have the higher ratings. With the exception of the no augmentation cases (nos. 4 and 7) the pilot ratings were generally acceptable for normal operation. Single-axis control with no augmentation was acceptable for emergency operation while three-axis no augmentation cases, which are not shown, were marginally controllable.

The rigid body bending moment performance shown in Fig. 18 is the maximum value attained during the trajectory. This normally occurred near the peak wind value. Except for the no augmentation cases, the loads encountered when flying the attitude stabilization task were comparable to those encountered with the vehicle under automatic control and for the wind used, slightly exceeded the design load. For the load reduction task, the loads were significantly reduced. The no augmentation cases indicate that with the wind used, loads are likely to exceed design values.

Figure 19 presents the maximum value of elastic body accelerations attained during the trajectory. They are presented as the component of acceleration at the pilot's station due to elastic motion for the pitch and yaw planes. Preliminary estimates indicate the structural stress contribution due to these accelerations to be negligible. It can be seen that except for the no augmentation cases the values are well below 0.1 g's. It is anticipated that these motions will have negligible effect on pilot control capabilities.

The trajectory dispersions at first staging are shown in Fig. 20. The dispersions for task 3, where the distances normal to the nominal trajectory were displayed to the pilot, are significantly lower. These distances were displayed on the small meters built into the left and top of the upper all-attitude indicator as shown in Fig. 6. The load control tasks had much larger dispersions than the attitude stabilization tasks since the vehicle is maneuvered through rather large attitude angles to reduce the aerodynamic angle of attack.

Figure 21 shows the maximum value of attitude rate obtained during the trajectory while Fig. 22 presents the maximum value of engine angle. The average engine angle (about $3/4^{o}$) was less than the maximums indicated, hence the thrust vectoring velocity penalty will be negligible.

The maximum values of attitude error are presented in Fig. 23. As expected the values for the load reduction tasks are much greater than those for attitude stabilization.

For reference, Fig. 24 shows the maximum angle of attack. While not too significant, since the aerodynamic load contribution to structural load is proportional to the product of dynamic pressure and angle

of attack, it is seen that values for the load reduction tasks are lower.

The results of Figs. 17 through 24 indicate that a manual control system can possess a high degree of flexibility. The pilot may choose to minimize structural load, trajectory dispersions, or attitude errors, as the situation requires. The relative results for task numbers 5 and 6 justify the addition of attitude error to the display panel. The results also show that for an emergency situation, single-axis control is possible for the no augmentation cases. With the present control system, three-axis, no augmentation control is questionable.

CONCLUSIONS

The following conclusions are based on preliminary fixed-base simulation results and may be modified after a more complete investigation.

(1) A piloted control system provides a high degree of flexibility and is capable of successfully completing the control tasks during the first stage of Saturn V boost.

(2) A significant problem area encountered is the design of the rate augmentation filter. Care must be taken to avoid adding lightly damped oscillatory modes to the system response at pilot control frequencies.

(3) Single-axis control can be completed without the aid of rate augmentation, while with the preliminary system developed for this study, three-axis control with no rate augmentation is marginal.

(4) Structural elastic bending motions sensed at the pilot's station are low enough in amplitude that they should not present a significant motion cue problem area.

(5) The three-axis side-arm controller and conventional aircraft instrumentation used were satisfactory.

Future studies will include the addition of motion cues and fuel sloshing modes to the simulation. An investigation of emergency situations will also be made as well as a more complete vehicle and control system parameter variation.

REFERENCES

1. Dragseth, G. K.: Feasibility of Piloted Boost Control. The Boeing Co., 1962. Paper presented at TBC Symposium, March 1962.

2. Dragseth, G. K.: D2-80762, Pilot in the Booster Loop Study - Final Report. The Boeing Co., December 1962.

3. Anon.: ER 11921 - Evaluation of Pilot Manual Control During Boost Flight. The Martin Co., November 1961.

4. Anon.: Er 12378 - Appendix I - Titan III Flight Control System Studies of Human Pilot Capability. The Martin Co., April 1962.

5. Holleman, E. C., Armstrong, N. A., and Andrews, W. H.: Utilization of the Pilot in Launch and Injection of a Multistage Orbital Vehicle. IAS 60-16. Paper presented at IAS 28th Annual Meeting, New York, January 25-27, 1960.

6. Anon.: IN-P and VE-V-62-6, C-5 Launch Vehicle Design Data. Marshall Space Flight Center, December 1962.

7. Cooper, G. E.: Understanding and Interpreting Pilot Opinion. Aero. Engr. Rev., March 1957.

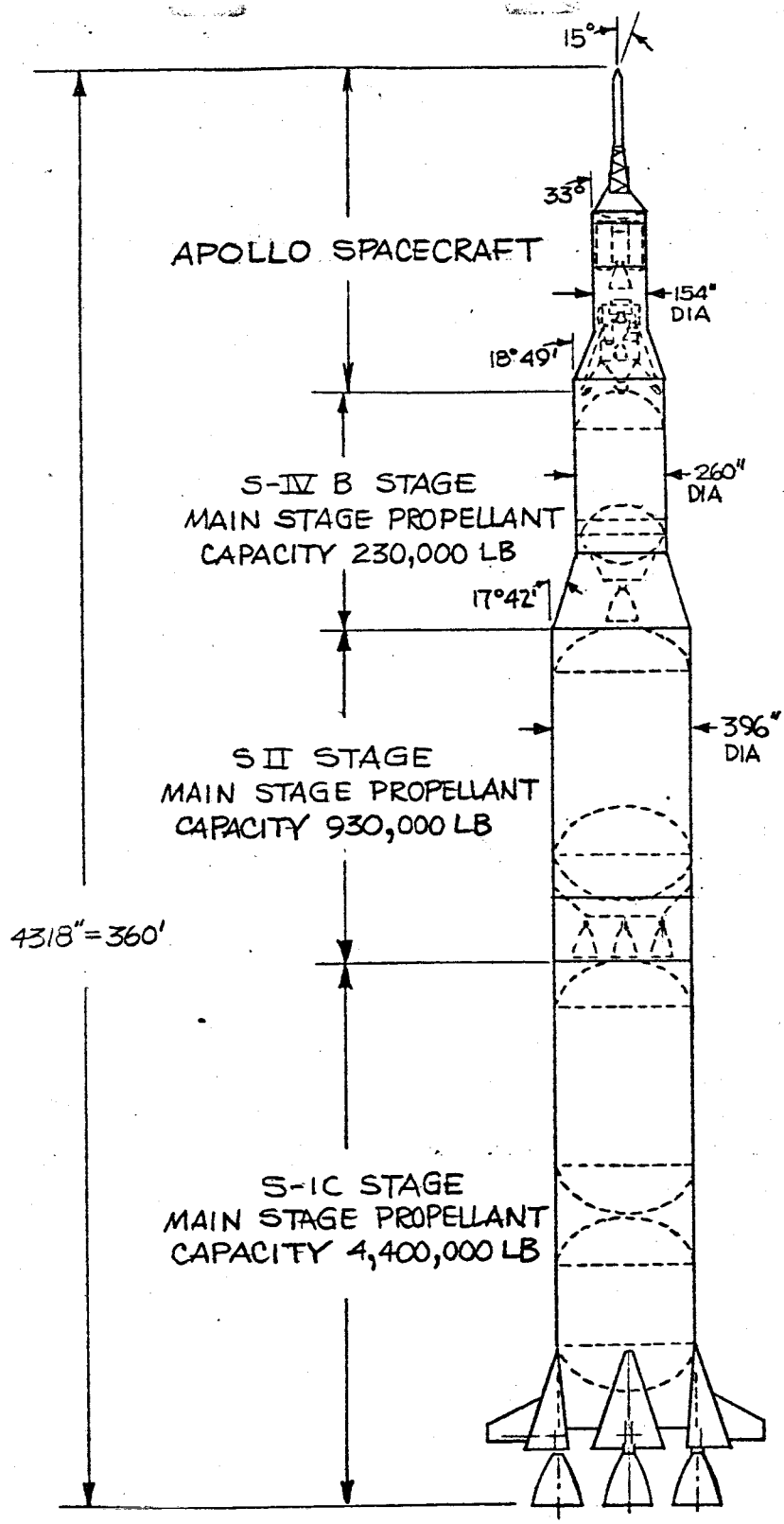

FIGURE 1 SATURN V VEHICLE CONFIGURATION

NASA
AMES RESEARCH CENTER

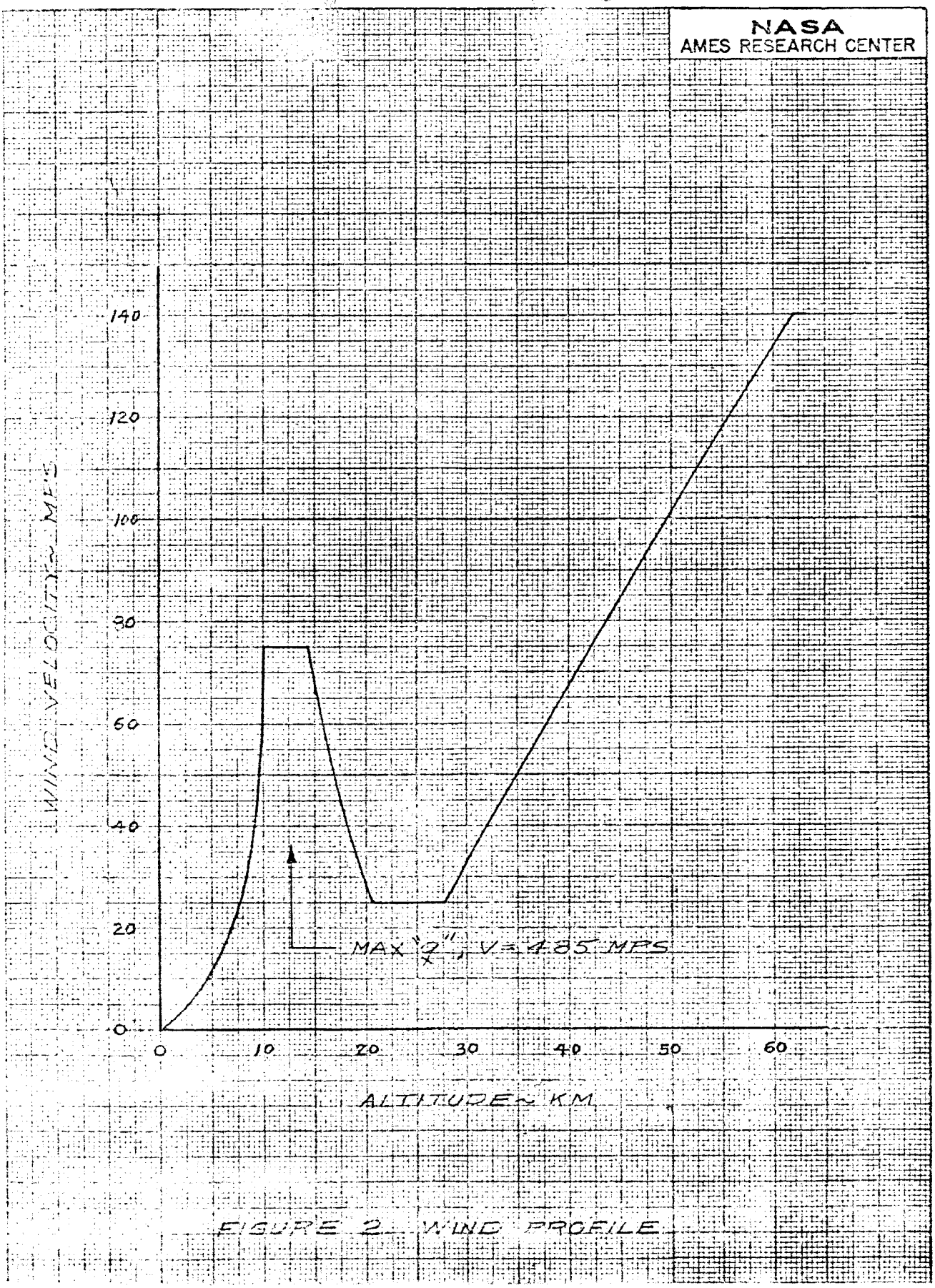

FIGURE 2 WIND PROFILE

PROPOSED PILOT OPINION RATING SYSTEM FOR UNIVERSAL USE

	ADJECTIVE RATING	NUMERICAL RATING	DESCRIPTION	PRIMARY MISSION ACCOMPLISHED?	BE[illegible]PED
NORMAL OPERATION	Satisfactory	1	Excellent, includes optimum	Yes	Yes
		2	Good, pleasant to fly	Yes	Yes
		3	Satisfactory, but with some mildly unpleasant characteristics	Yes	Yes
EMERGENCY OPERATION	Unsatisfactory	4	Acceptable, but with unpleasant characteristics	Yes	Yes
		5	Unacceptable for normal operation	Doubtful	Yes
		6	Acceptable for emergency condition only*	Doubtful	Yes
NO OPERATION	Unacceptable	7	Unacceptable even for emergency condition *	No	Doubtful
		8	Unacceptable - dangerous	No	No
		9	Unacceptable - uncontrollable	No	No
	Unprintable	10	x!◎ɯɯɯɯ!! Did not get back to report	What mission?	

*(Failure of a stability augmenter)

Figure 3 – Rating scale

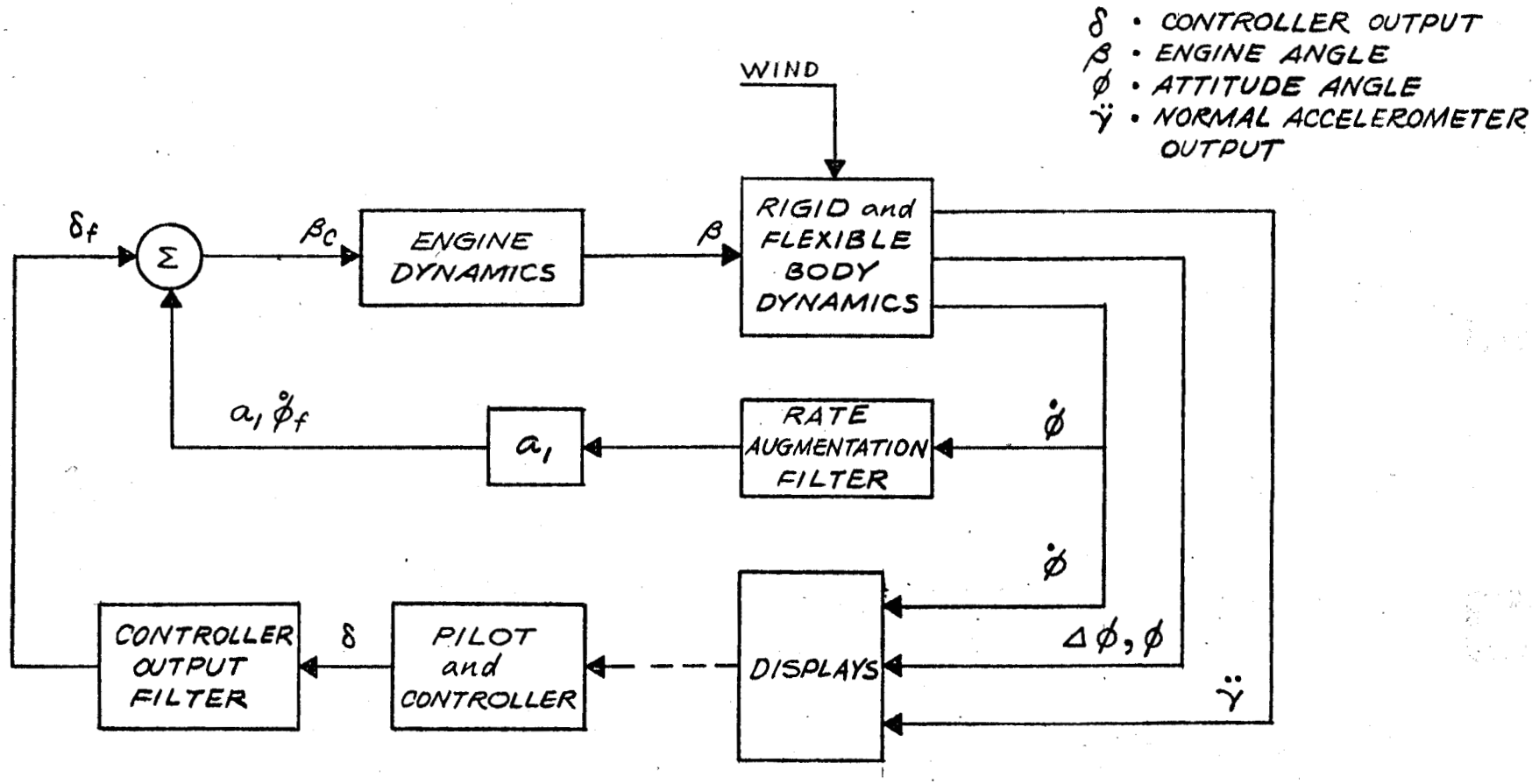

FIGURE 4 - PITCH, YAW, PRELIMINARY PRIMARY MANUAL CONTROL SYSTEM.

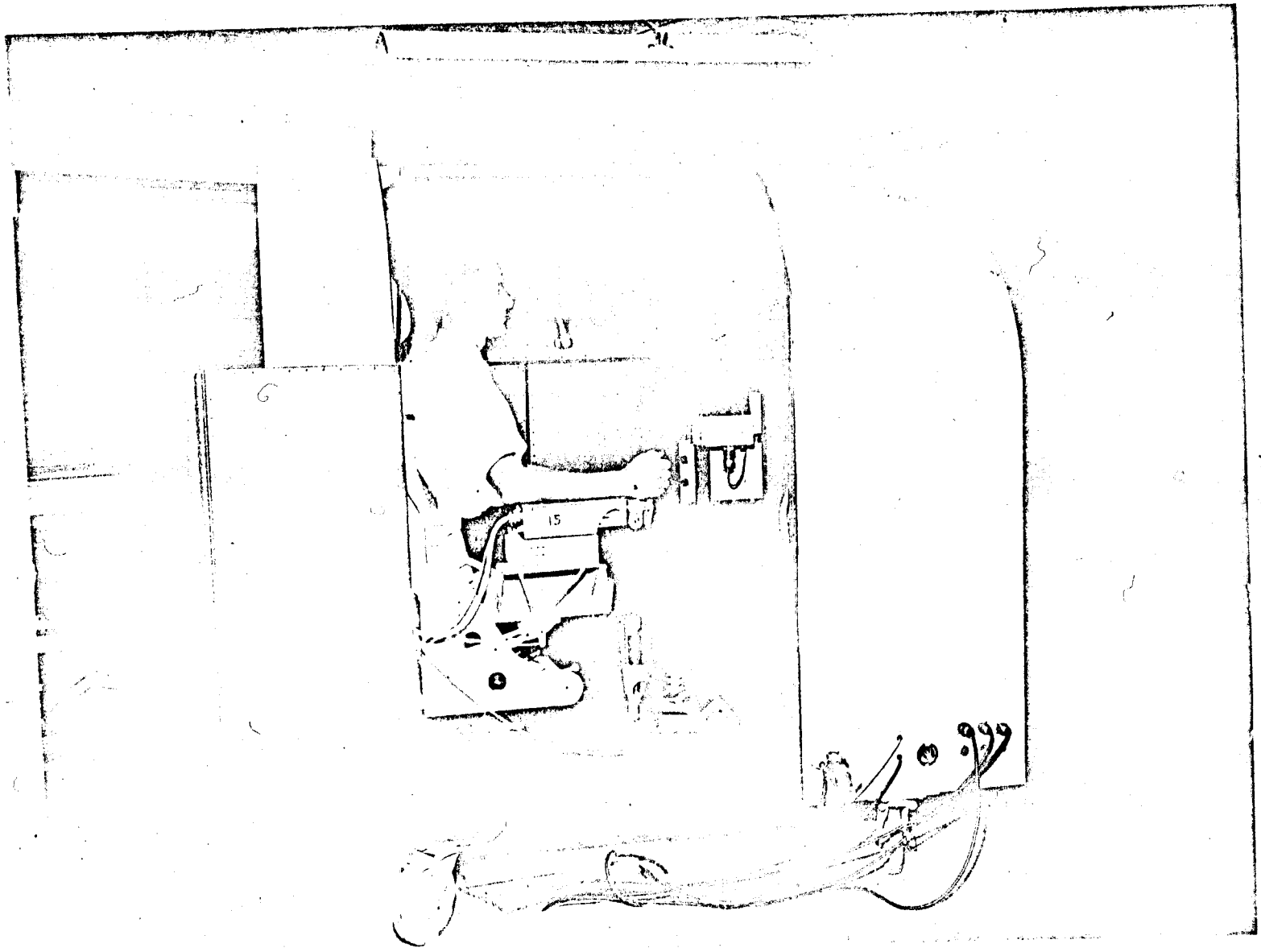

Figure 5 – Fixed base simulator

NATIONAL AERONAUTICS AND SPACE ADMINISTRATION
AMES RESEARCH CENTER, MOFFETT FIELD, CALIFORNIA

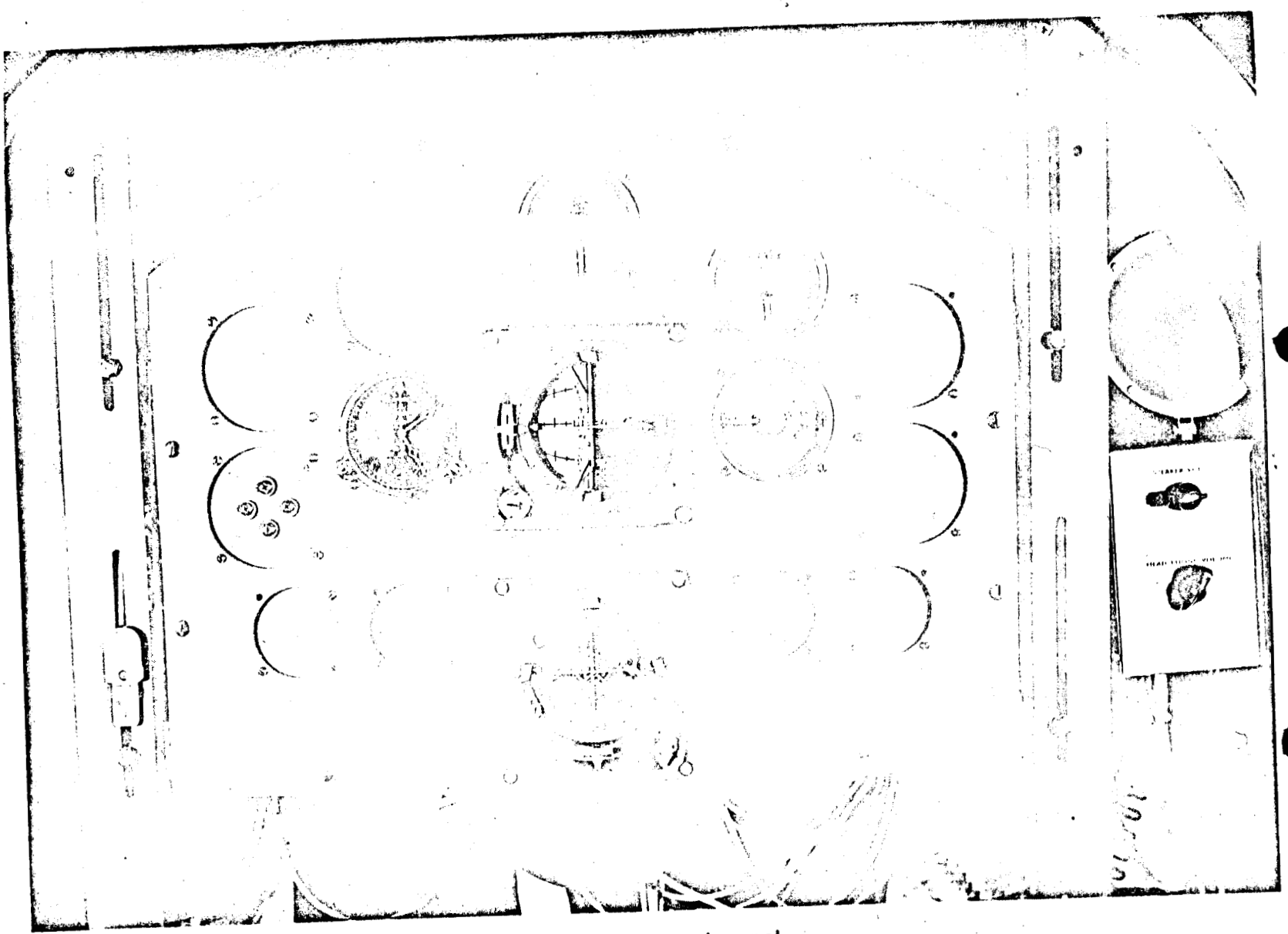

Figure 6—Instrument panel

NATIONAL AERONAUTICS AND SPACE ADMINISTRATION
AMES RESEARCH CENTER, MOFFETT FIELD, CALIFORNIA

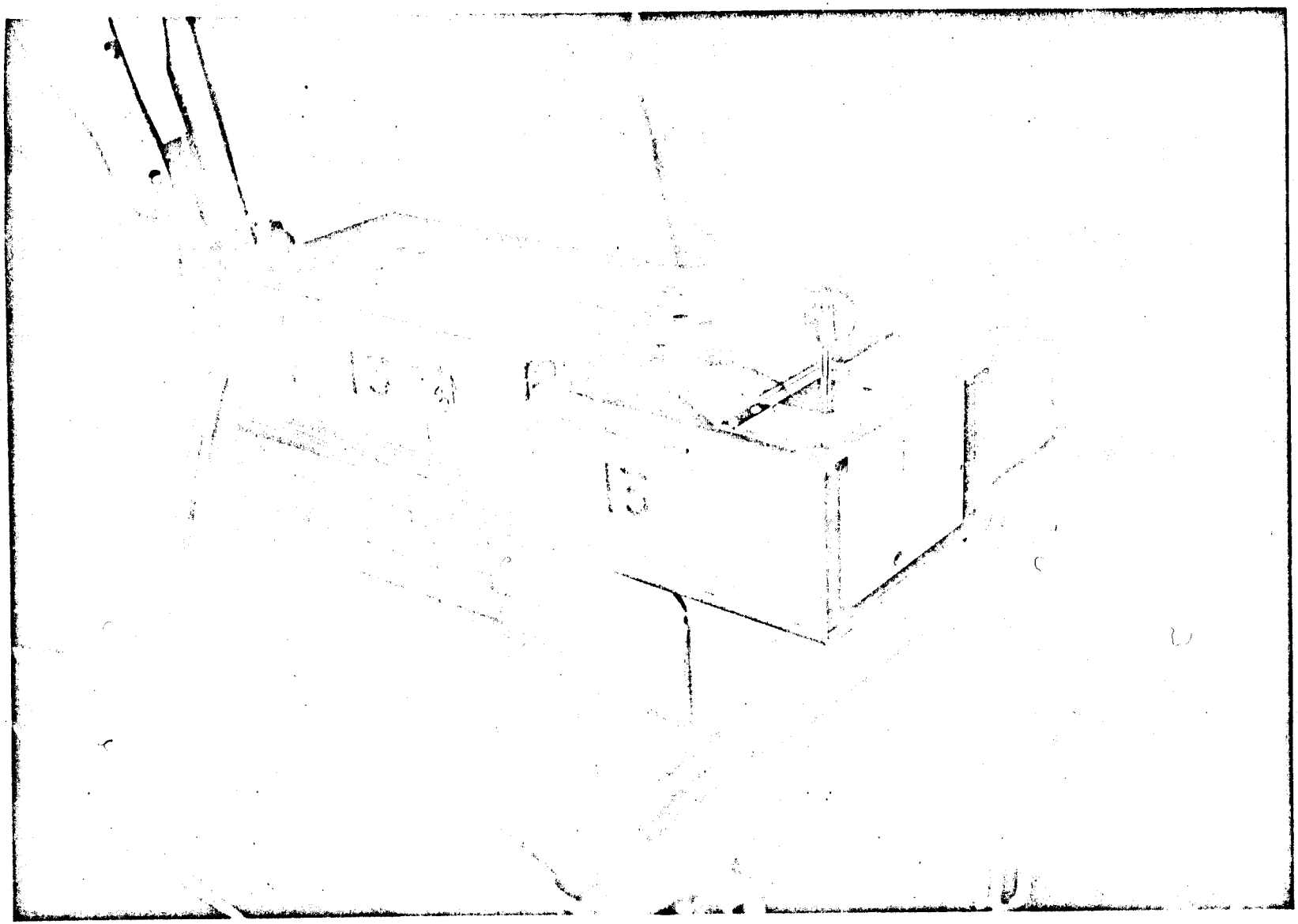

Figure 7—Two axis side arm controller

NATIONAL AERONAUTICS AND SPACE ADMINISTRATION
AMES RESEARCH CENTER, MOFFETT FIELD, CALIFORNIA

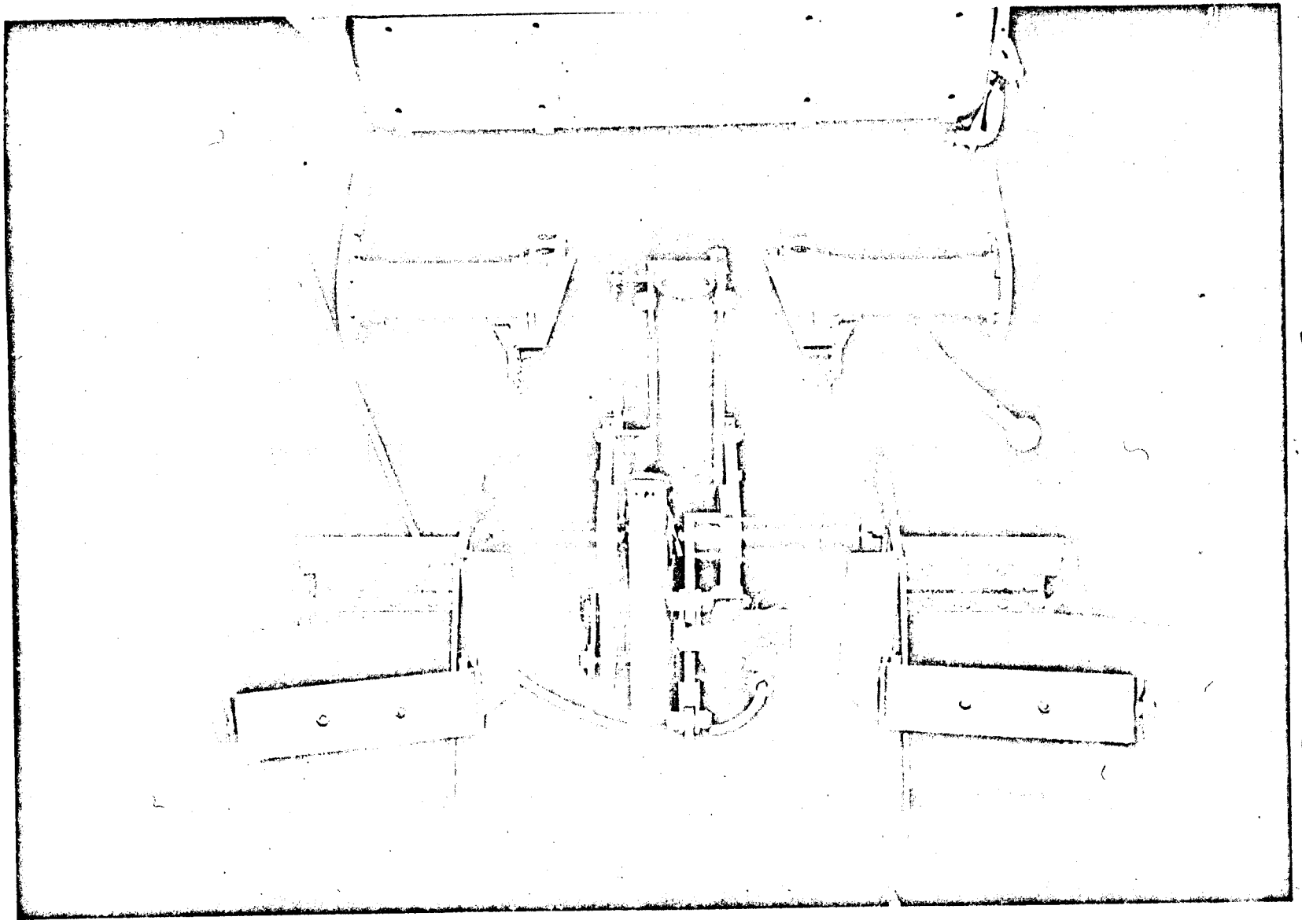

Figure 8 – Rudder pedals

NATIONAL AERONAUTICS AND SPACE ADMINISTRATION
AMES RESEARCH CENTER, MOFFETT FIELD, CALIFORNIA

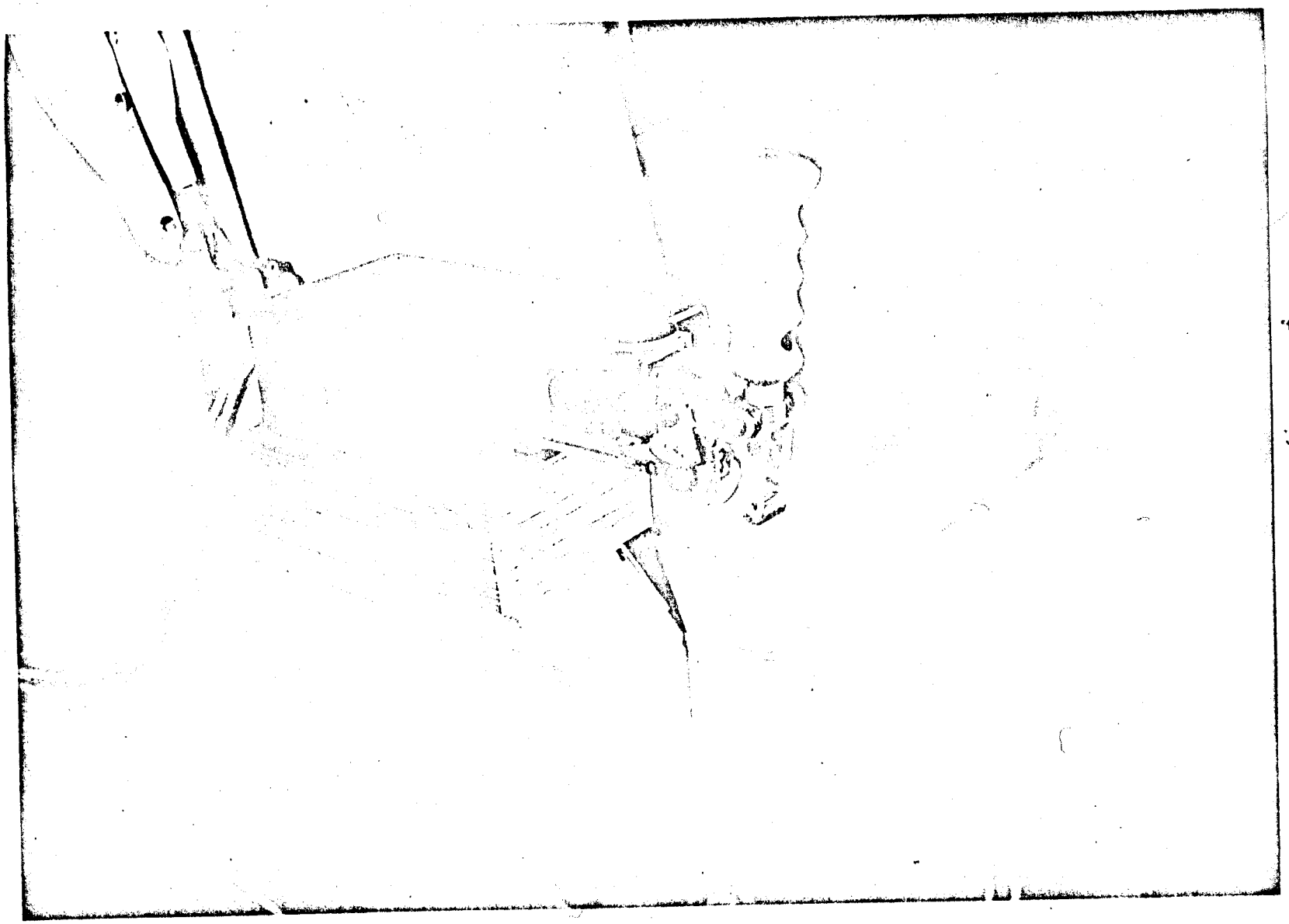

Figure 9 – Three axis side arm controller

NATIONAL AERONAUTICS AND SPACE ADMINISTRATION
AMES RESEARCH CENTER, MOFFETT FIELD, CALIFORNIA

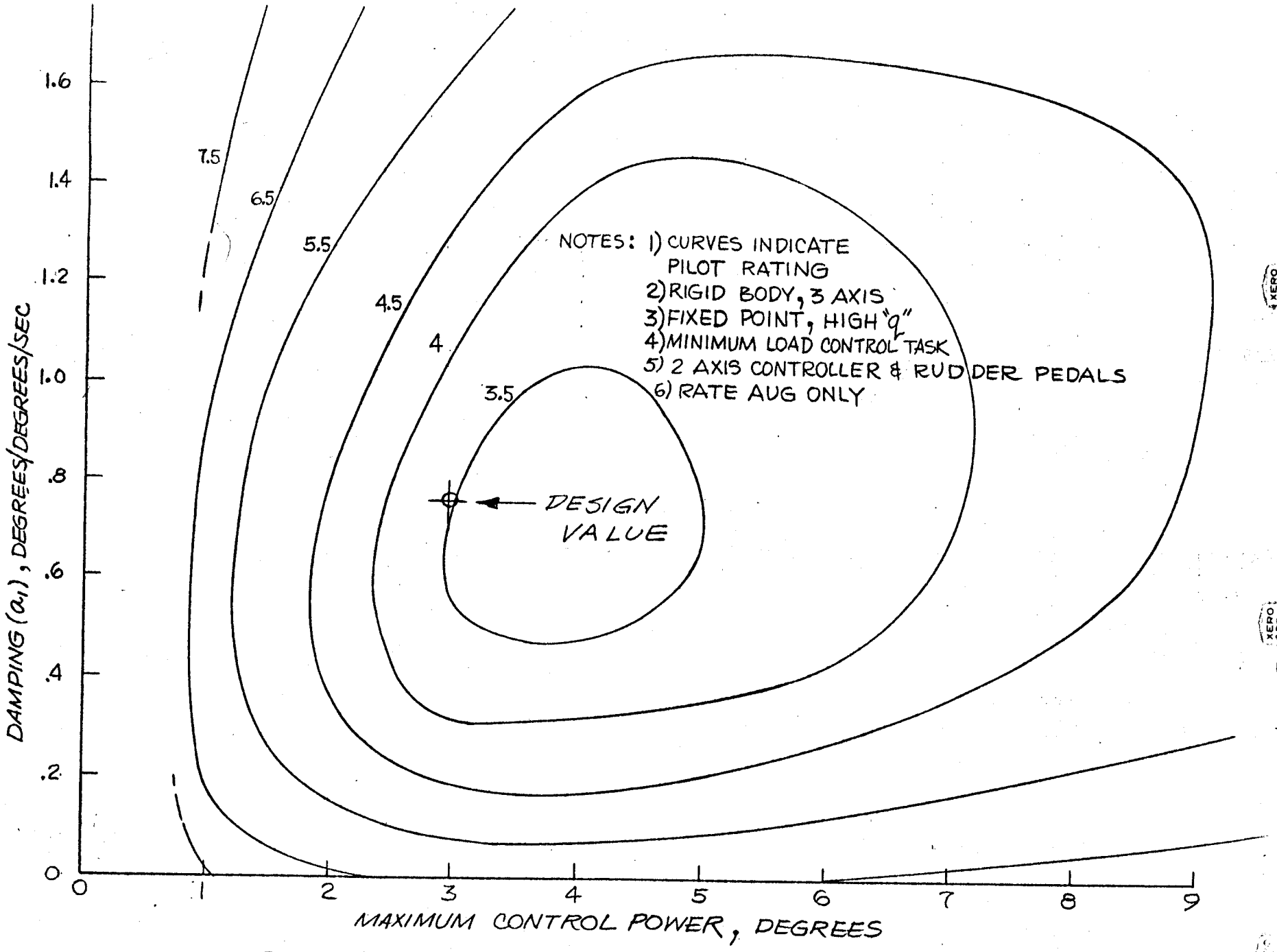

FIGURE 10 – PILOTED BOOST CONTROL BOUNDARIES

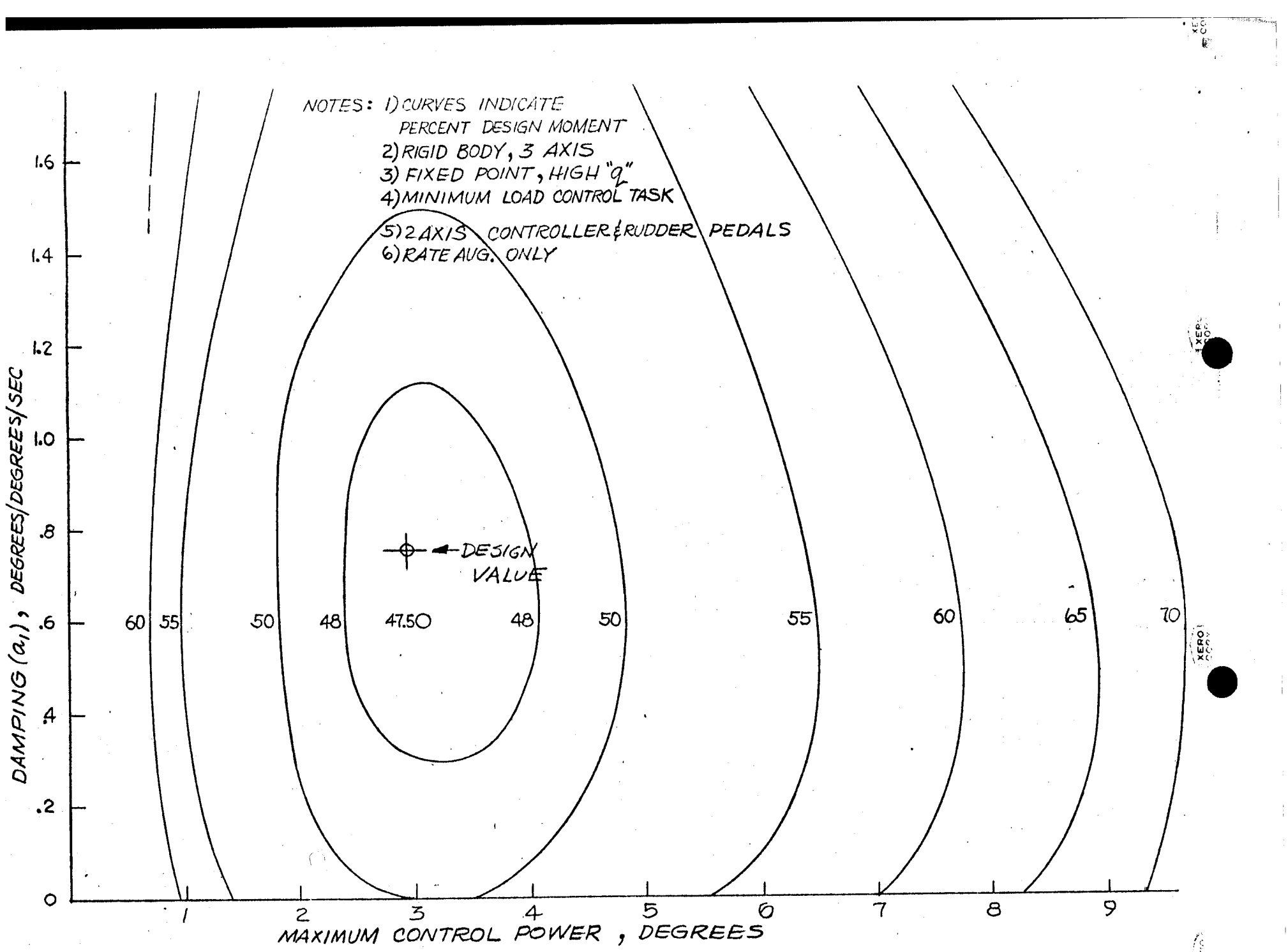

FIGURE 11 – PILOTED BOOST PERFORMANCE

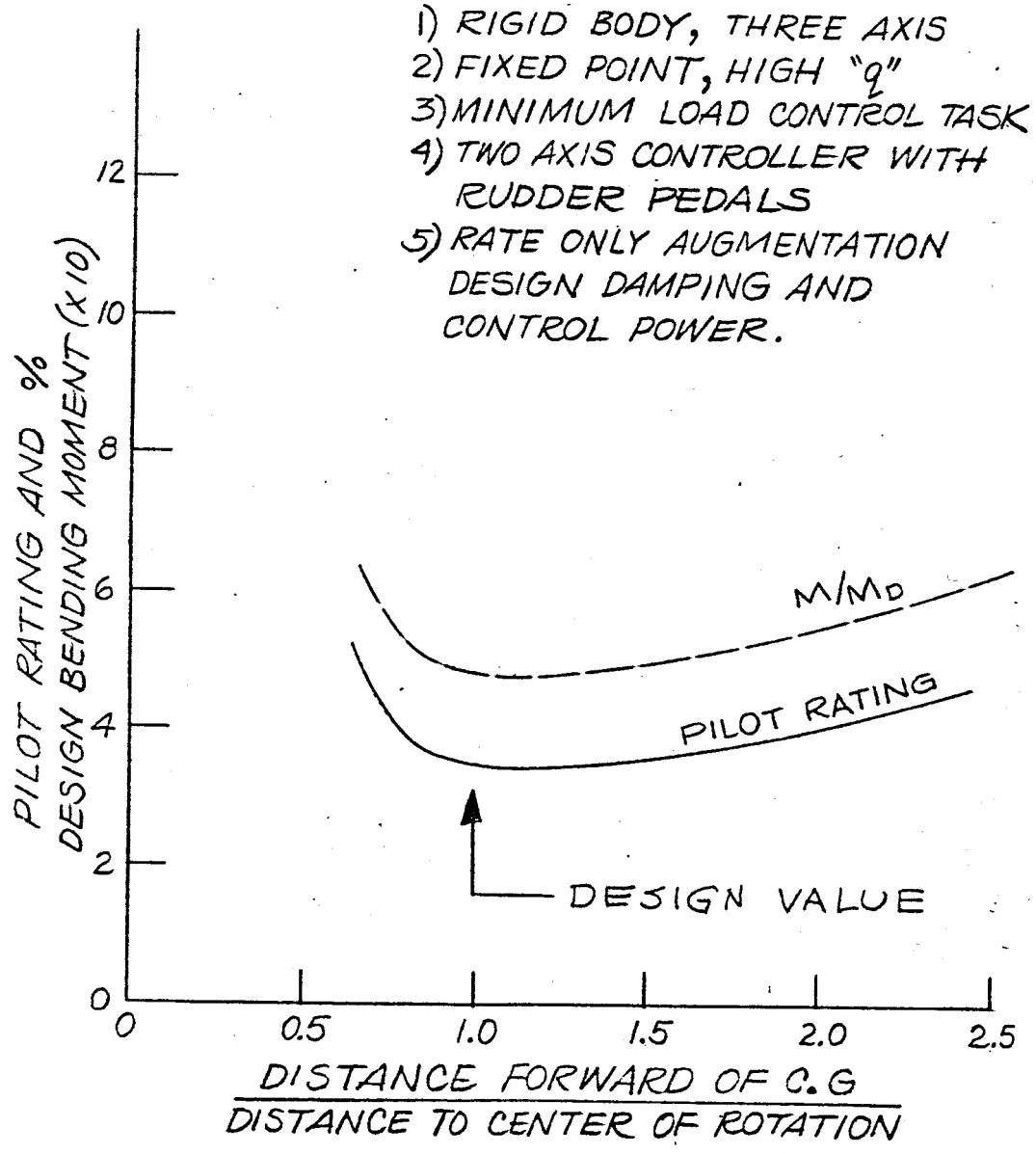

FIGURE 12. DISPLAY ACCELEROMETER LOCATION

ACCELEROMETER AUGMENTATION

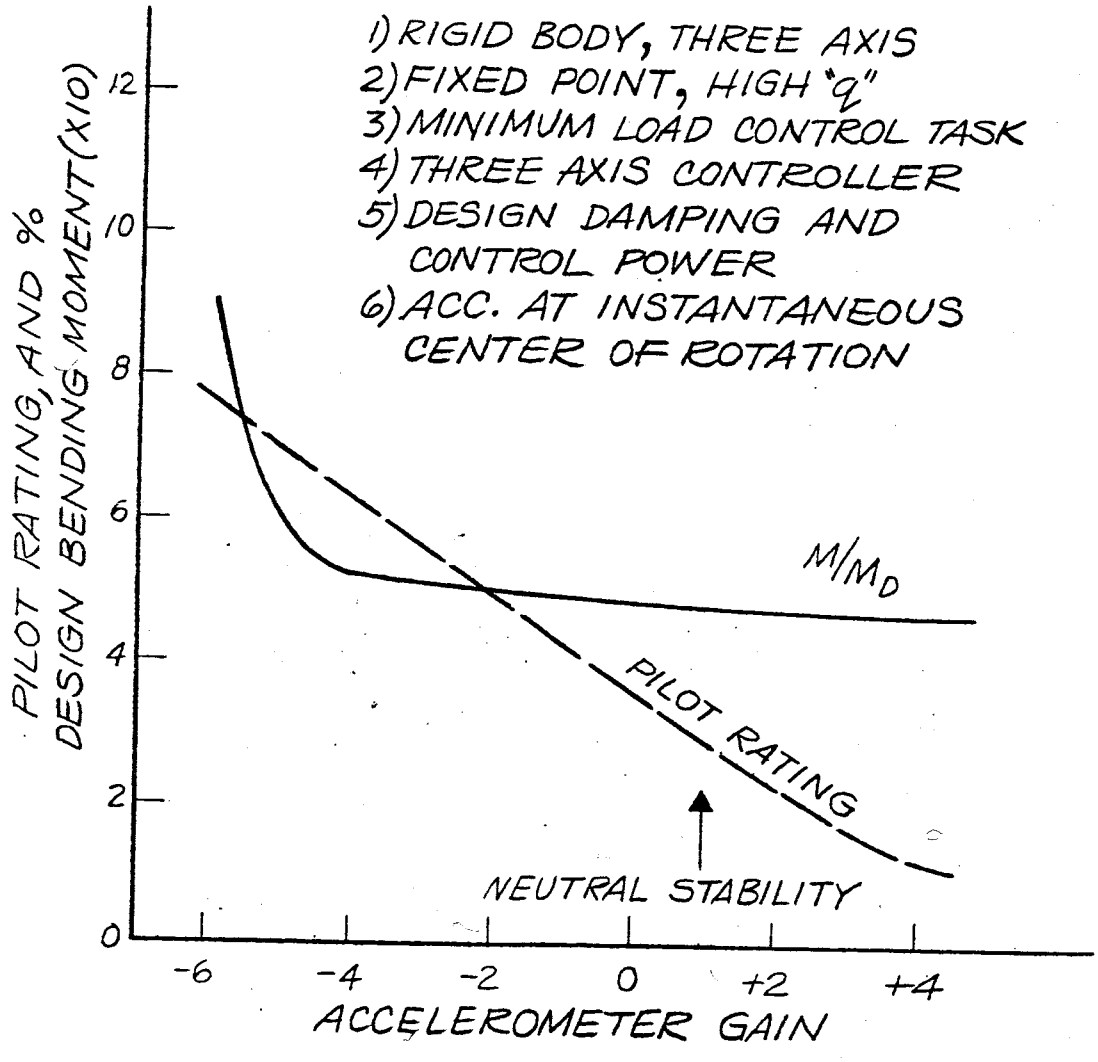

FIGURE 13 ACCELEROMETER AUGMENTATION

CONTROLLER FILTER

1) FLEXIBLE BODY, SINGLE AXIS
2) FIXED POINT, HIGH "q"
3) MINIMUM LOAD CONTROL TASK
4) THREE AXIS CONTROLLER
5) DESIGN DAMPING AND CONTROL POWER
6) AUGMENTATION FILTER IN
7) NO DISPLAY FILTER
8) SECOND ORDER CONTROLLER FILTER WITH $\mathcal{L}_C = 0.5$

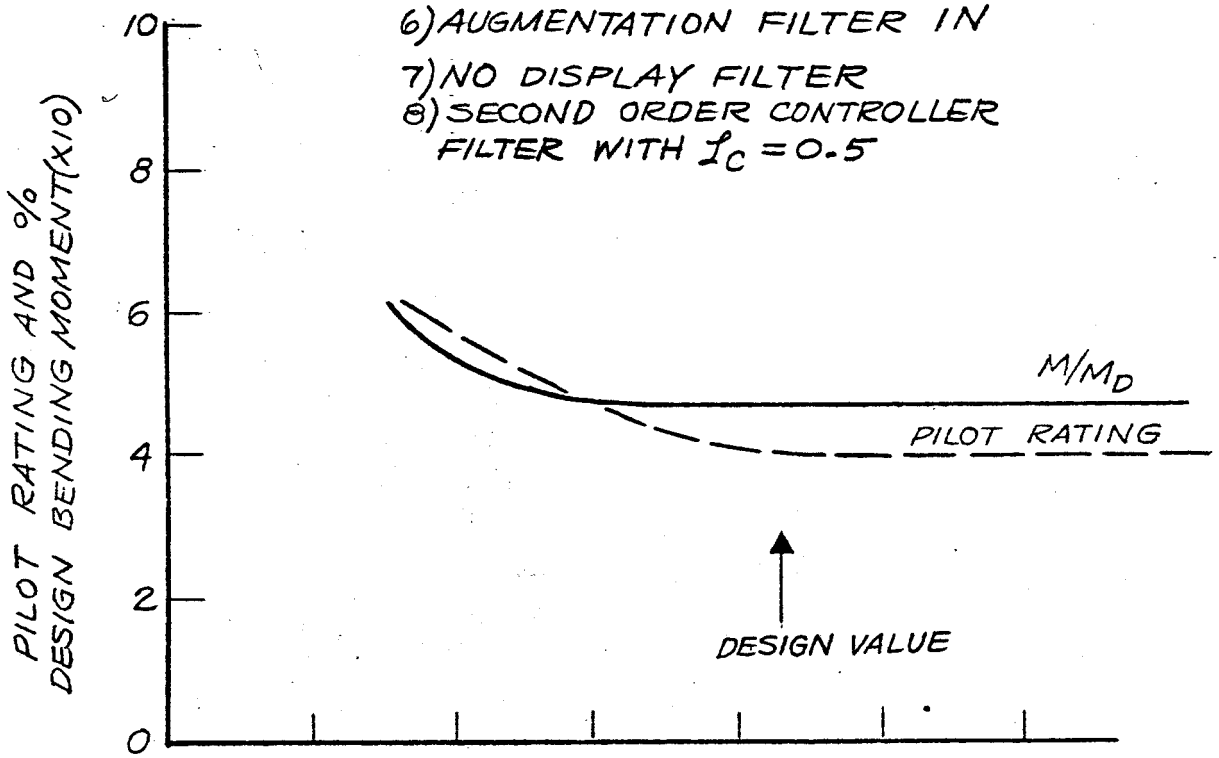

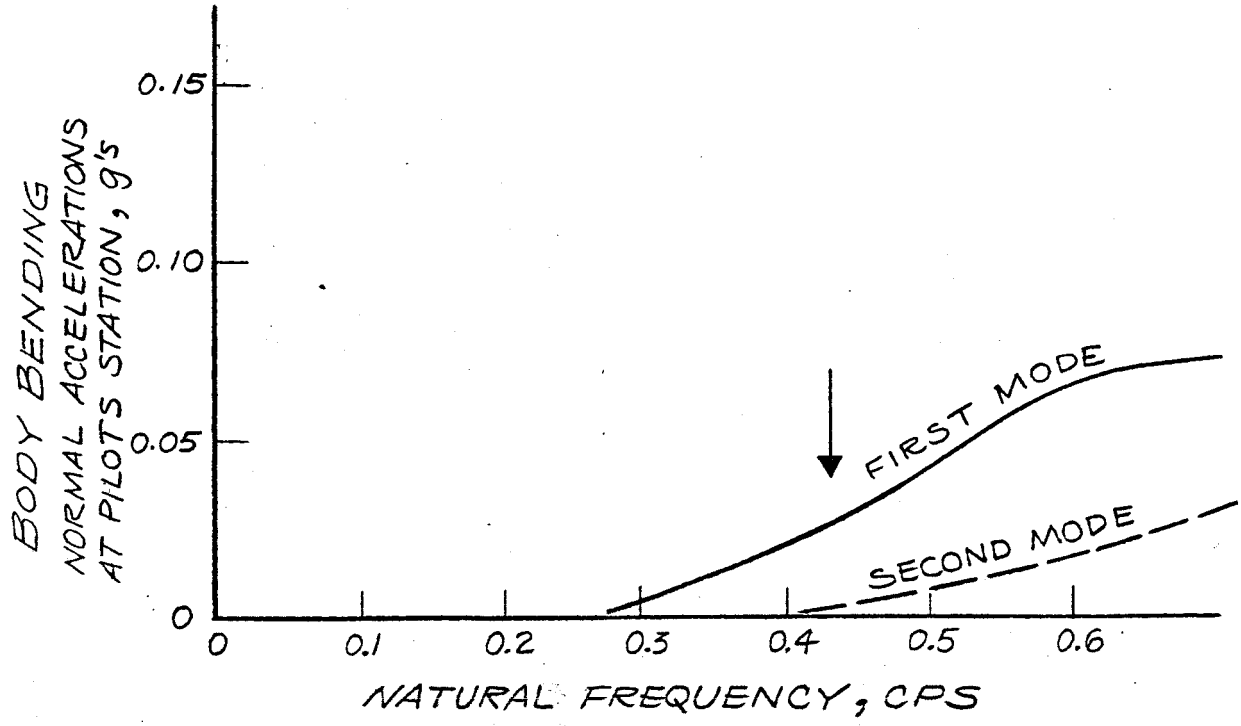

FIGURE 14 CONTROLLER FILTER

1) FLEXIBLE BODY, SINGLE AXIS
2) FIXED POINT, FIRST
3) MINIMUM LOAD CONTROL TASK
4) THREE AXIS CONTROLLER
5) DESIGN DAMPING AND CONTROL POWER
6) AUGMENTATION FILTER IN
7) NO DISPLAY FILTER
8) SECOND ORDER CONTROLLER FILTER WITH $\omega_{n_c} = .43$ cps, $\zeta_c = 0.5$

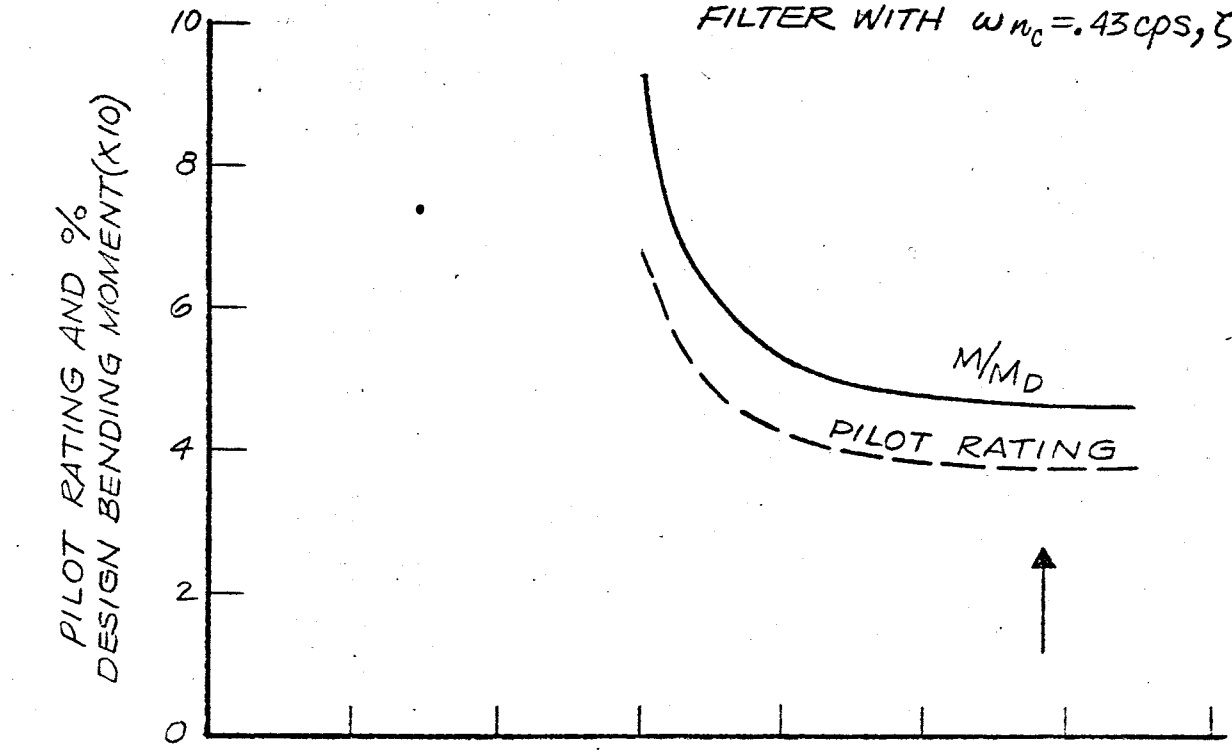

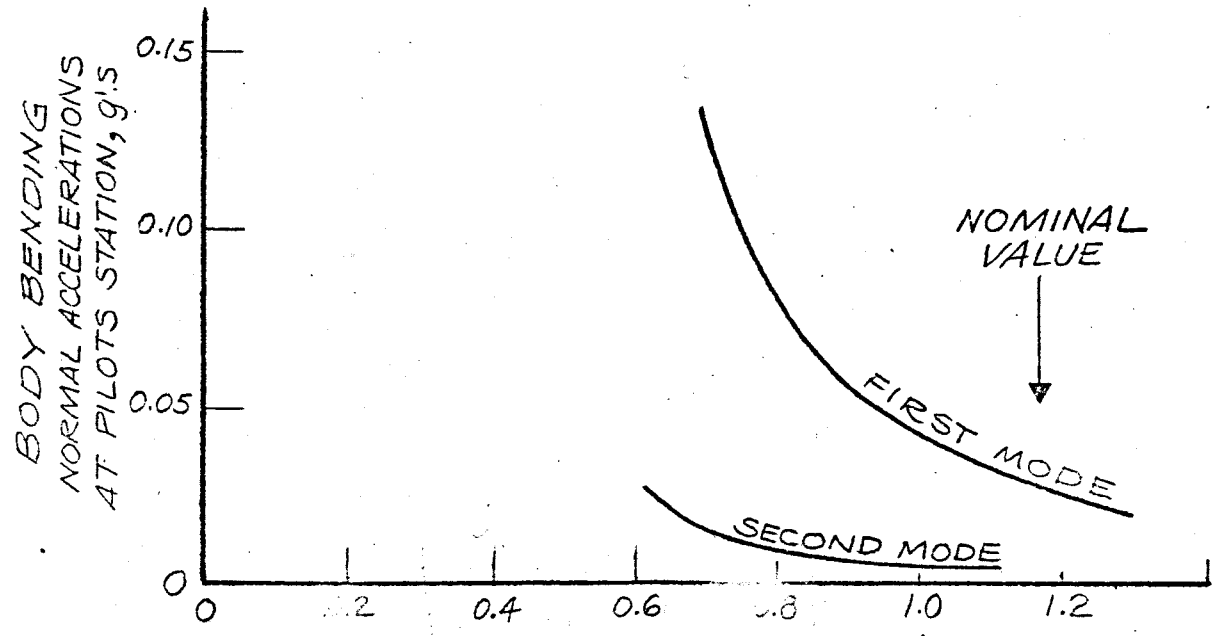

FIGURE 15 SYSTEM SENSITIVITY

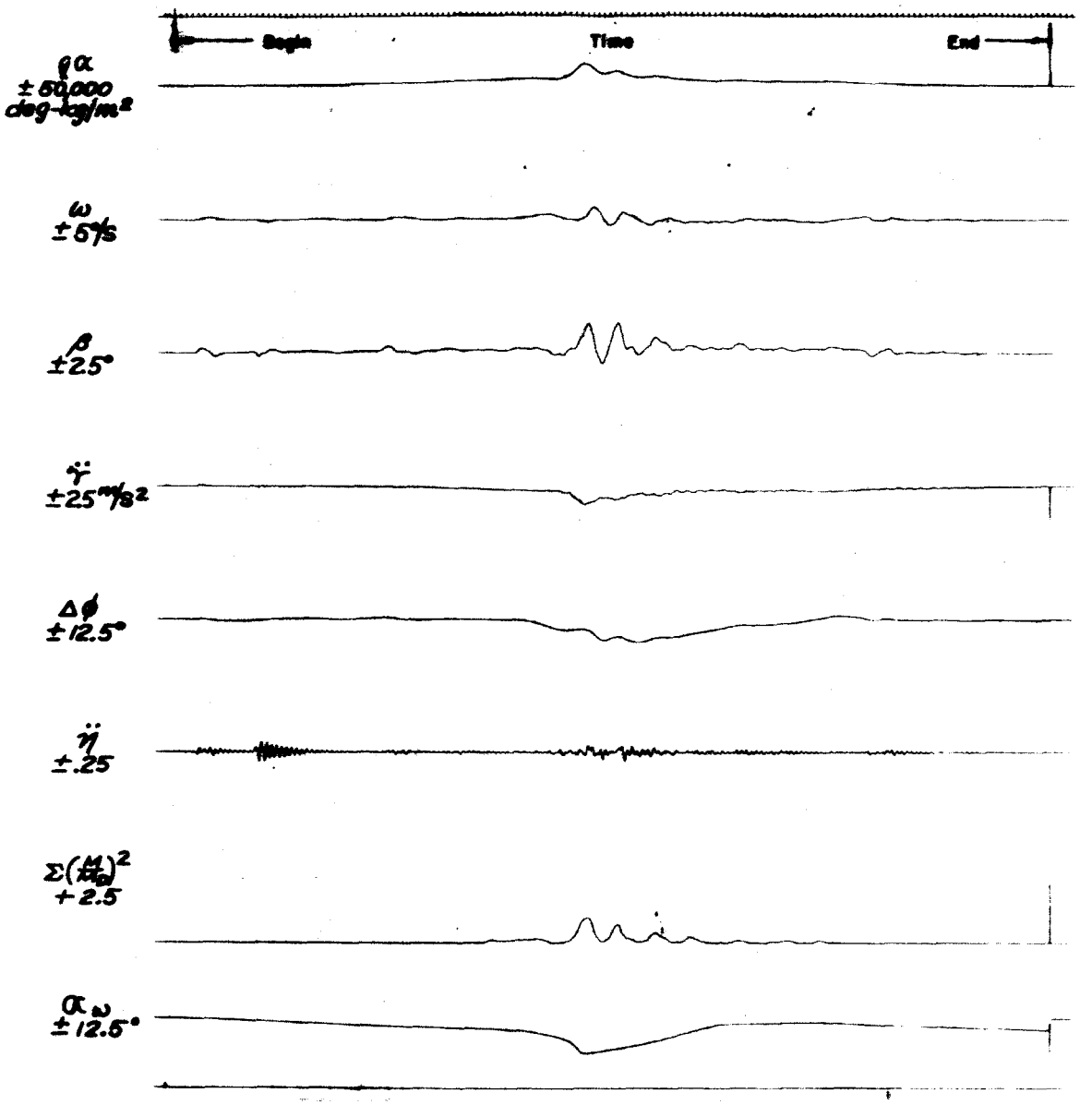

Figure 18.— Typical run

ϕ · ATTITUDE ANGLE
$\Delta\phi$ · ATTITUDE ERROR
$\dot{\phi}$ · ATTITUDE RATE
X · ATTITUDE PROGRAM
$\ddot{r}$ · NORMAL ACCELEROMETER OUTPUT

1) THREE AXIS CONTROLLER
2) DAMPING, $a_1 = 0.75$
3) MAXIMUM CONTROL POWER, 3.5 deg/sec^2
4) CONTROLLER FILTER, $\omega_n = 2.7$ rad/sec, $\zeta = 0.5$

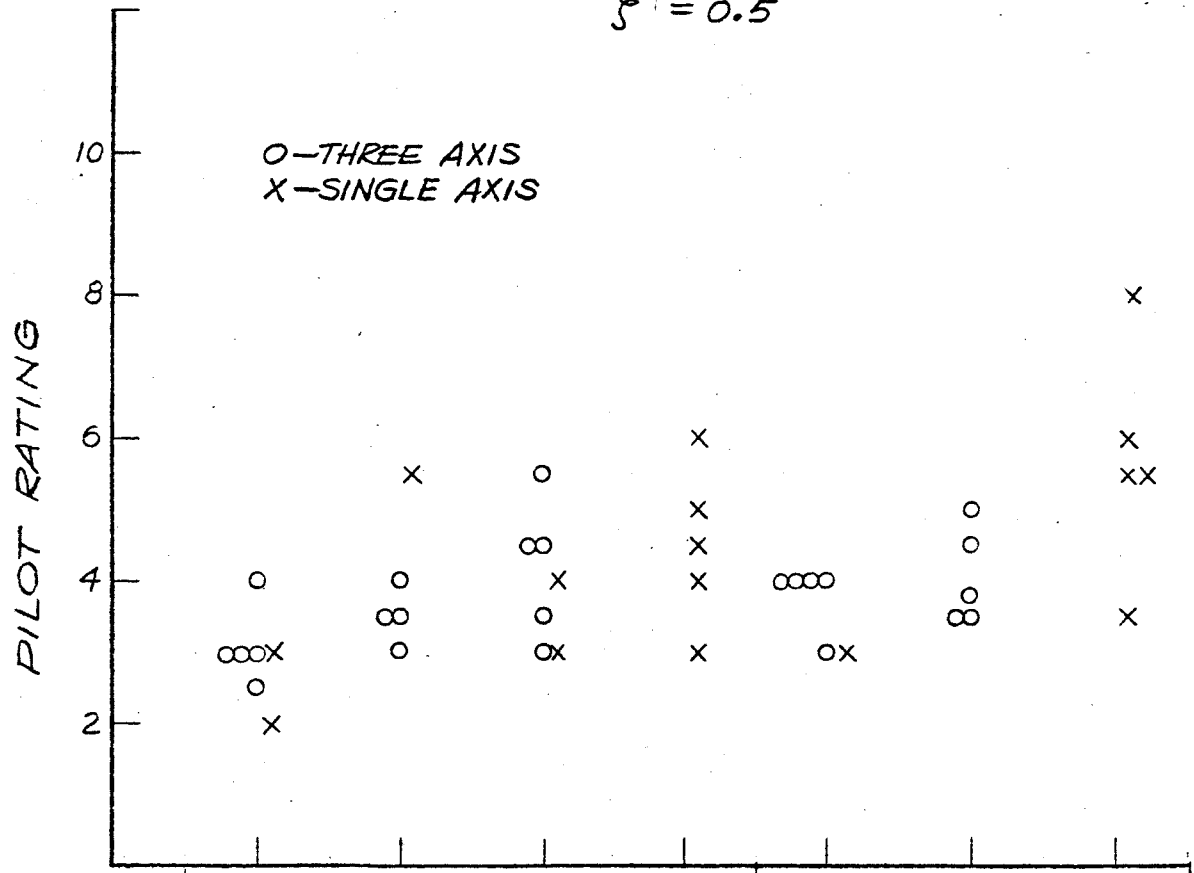

PRIMARY TASK	ATTITUDE STAB.				LOAD CONTROL		
SECONDARY TASK		TRAJ. DISPERSION		RATE			RATE
PRIMARY DISPLAY	$\Delta\phi$	$\Delta\phi$	$\Delta\phi$	$\Delta\phi$	$\Delta\phi, \ddot{r}$	$\phi, X, \ddot{r}$	$\Delta\phi, \ddot{r}$
SECONDARY DISPLAY		$\ddot{r}$	$\ddot{r}, X$	$\dot{\phi}$			$\dot{\phi}$
TASK NUMBER	1	2	3	4	5	6	7

FIGURE 17 PILOT RATING

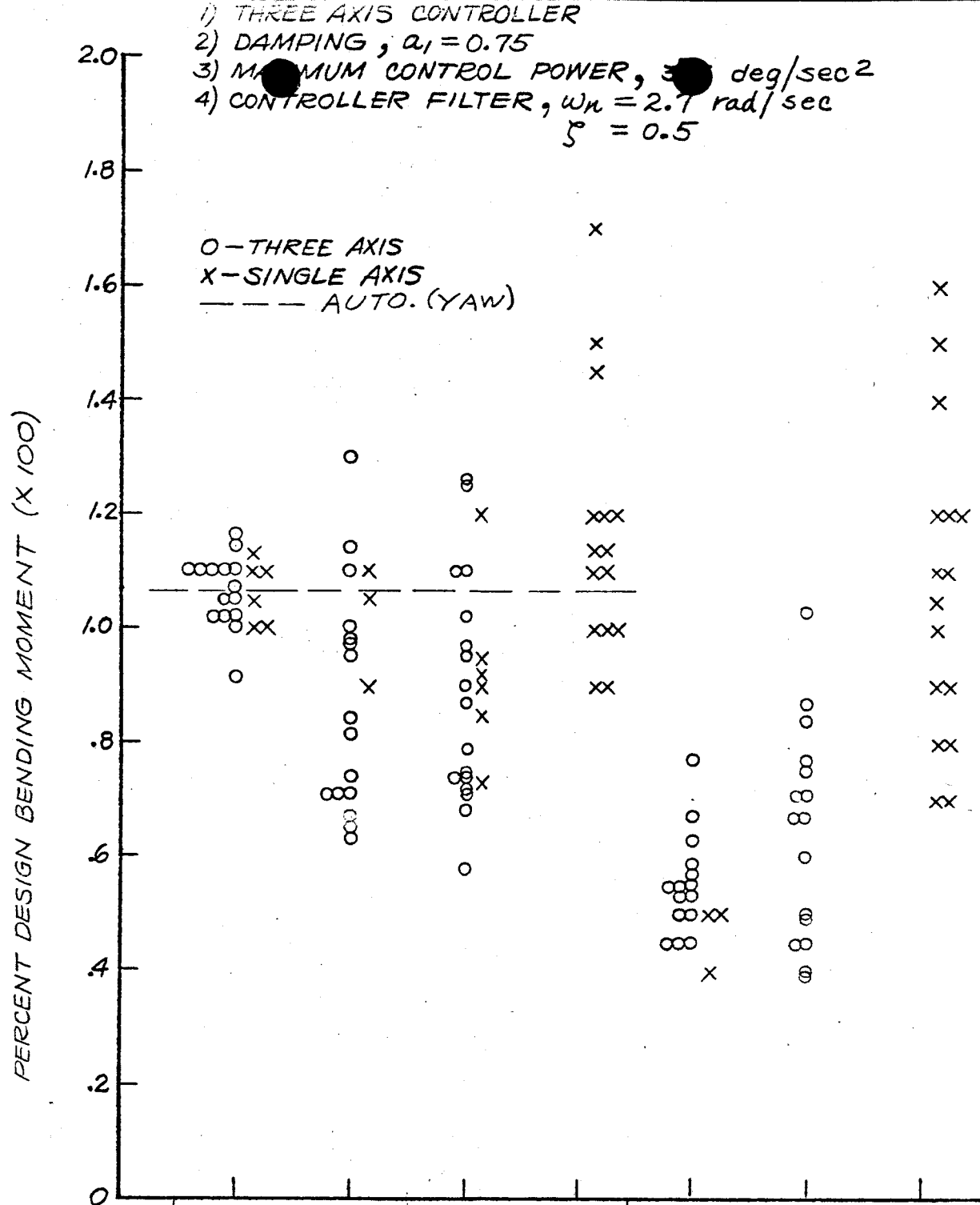

PRIMARY TASK	ATTITUDE STAB				LOAD CONTROL		
SECONDARY TASK		TRAJ. DISPERSION					RATE
PRIMARY DISPLAY	$\Delta\phi$	$\Delta\phi$	$\Delta\phi$	$\Delta\phi$	$\Delta\phi, \ddot{\gamma}$	$\phi, x, \ddot{\gamma}$	$\Delta\phi, \ddot{\gamma}$
SECONDARY DISPLAY		$\ddot{\gamma}$	$\ddot{\gamma}, x$	$\dot{\phi}$			$\dot{\phi}$
TASK NUMBER	1	2	3	4	5	6	7

FIGURE 18 RIGID BODY BENDING MOMENT

1) THREE AXIS CONTROLLER
2) DAMPING, $a_1 = 0.75$
3) MAXIMUM CONTROL POWER, 3.5 deg/sec^2
4) CONTROLLER FILTER, $\omega_n = 2.7$ rad/sec
$\zeta = 0.5$

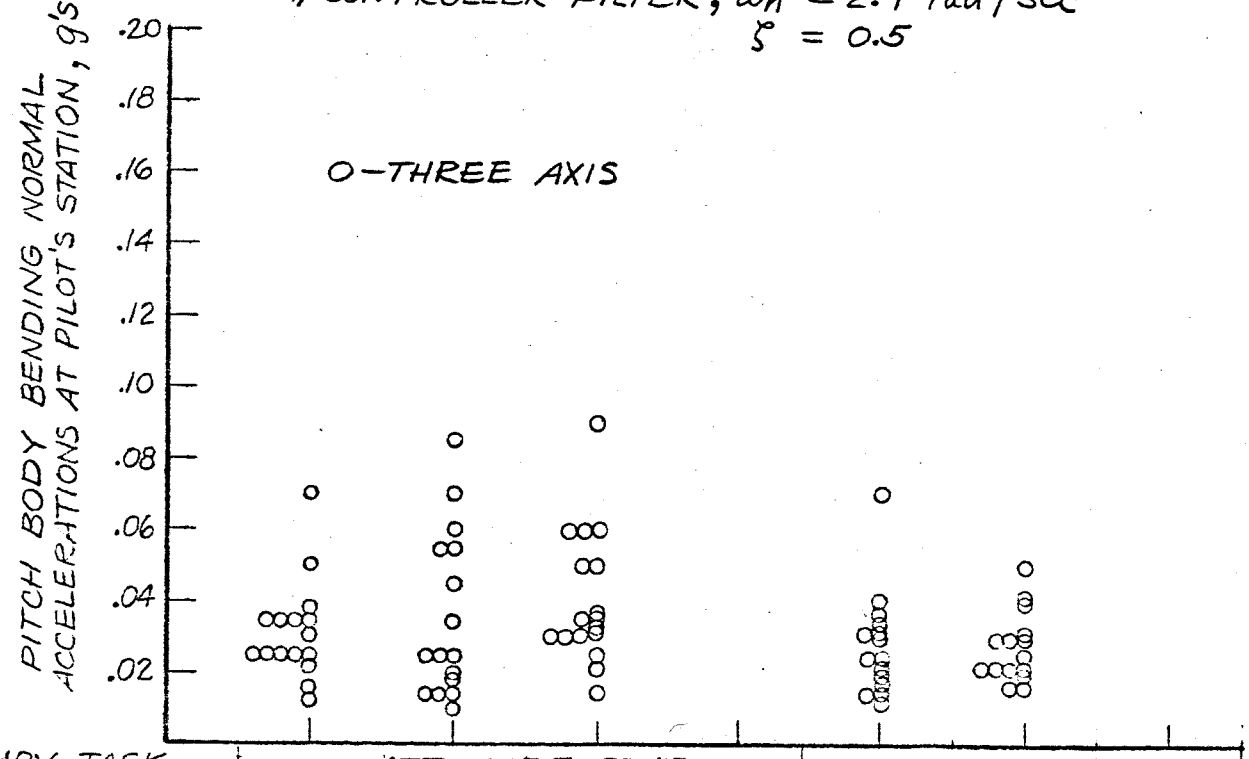

PRIMARY TASK	ATTITUDE STAB.				LOAD CONTROL		
SECONDARY TASK		TRAJ. DISPERSION		RATE			RATE
PRIMARY DISPLAY	$\Delta\phi$	$\Delta\phi$	$\Delta\phi$	$\Delta\phi$	$\Delta\phi, \ddot{\gamma}$	$\phi, x, \ddot{\gamma}$	$\Delta\phi, \ddot{\gamma}$
SECONDARY DISPLAY		$\ddot{\gamma}$	$\ddot{\gamma}, x$	$\ddot{\phi}$			$\ddot{\phi}$
TASK NUMBER	1	2	3	4	5	6	7

FIGURE 190 FLEXIBLE BODY NORMAL ACCELERATIONS

1) THREE AXIS CONTROLLER
2) DAMPING, $a_1 = 0.75$
3) MAXIMUM CONTROL POWER, 3.5 deg/sec^2
4) CONTROLLER FILTER, $\omega_n = 2.7$ rad/sec, $\zeta = 0.5$

O - THREE AXIS
X - SINGLE AXIS

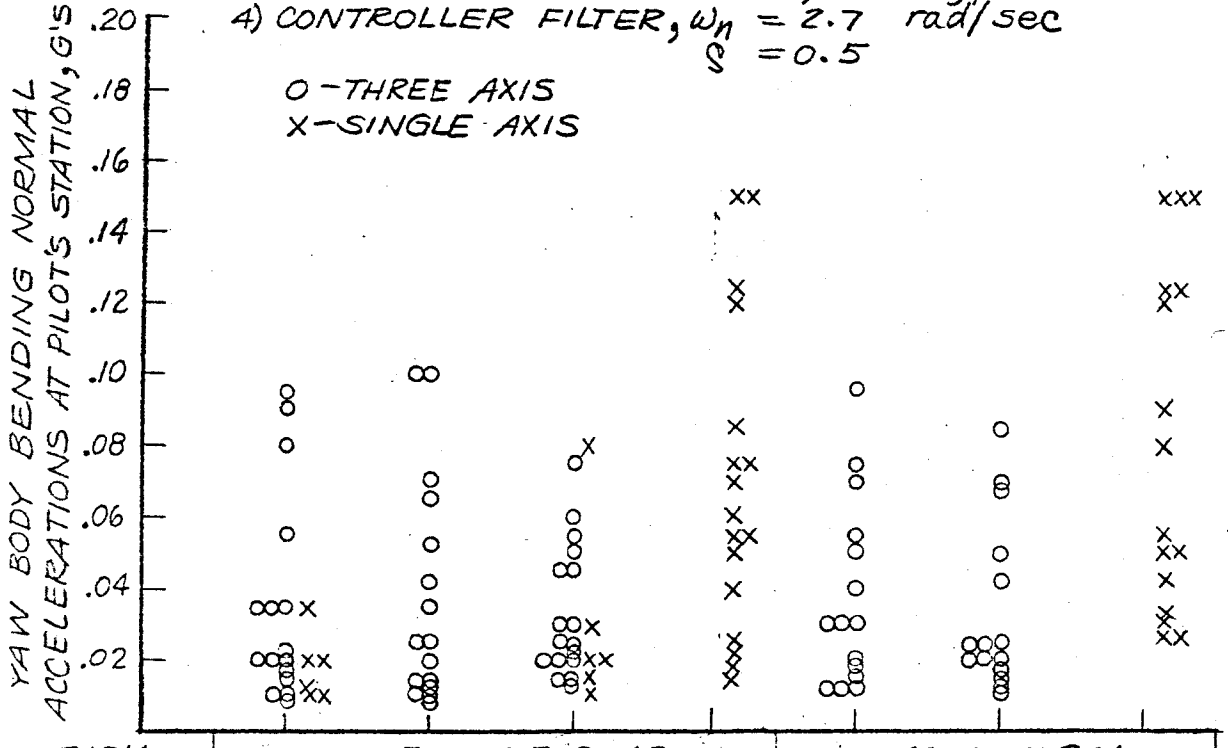

PRIMARY TASK	ATTITUDE STAB.				LOAD CONTROL		
SECONDARY TASK		TRAJ. DISPERSION		RATE			RATE
PRIMARY DISPLAY	$\Delta\phi$	$\Delta\phi$	$\Delta\phi$	$\Delta\phi$	$\Delta\phi, \ddot{r}$	$\phi, x, \ddot{r}$	$\Delta\phi, \ddot{r}$
SECONDARY DISPLAY		$\ddot{r}$	$\ddot{r}, x$	$\dot{\phi}$			$\dot{\phi}$
TASK NUMBER	1	2	3	4	5	6	7

FIGURE 196 FLEXIBLE BODY NORMAL ACCELERATIONS

1) THREE AXIS CONTROLLER
2) DAMPING, $\alpha_1 = 0.75$
3) MAXIMUM CONTROL POWER, 3.5 deg/sec^2
4) CONTROLLER FILTER, $\omega_n = 2.7$ rad/sec
$\zeta = 0.5$

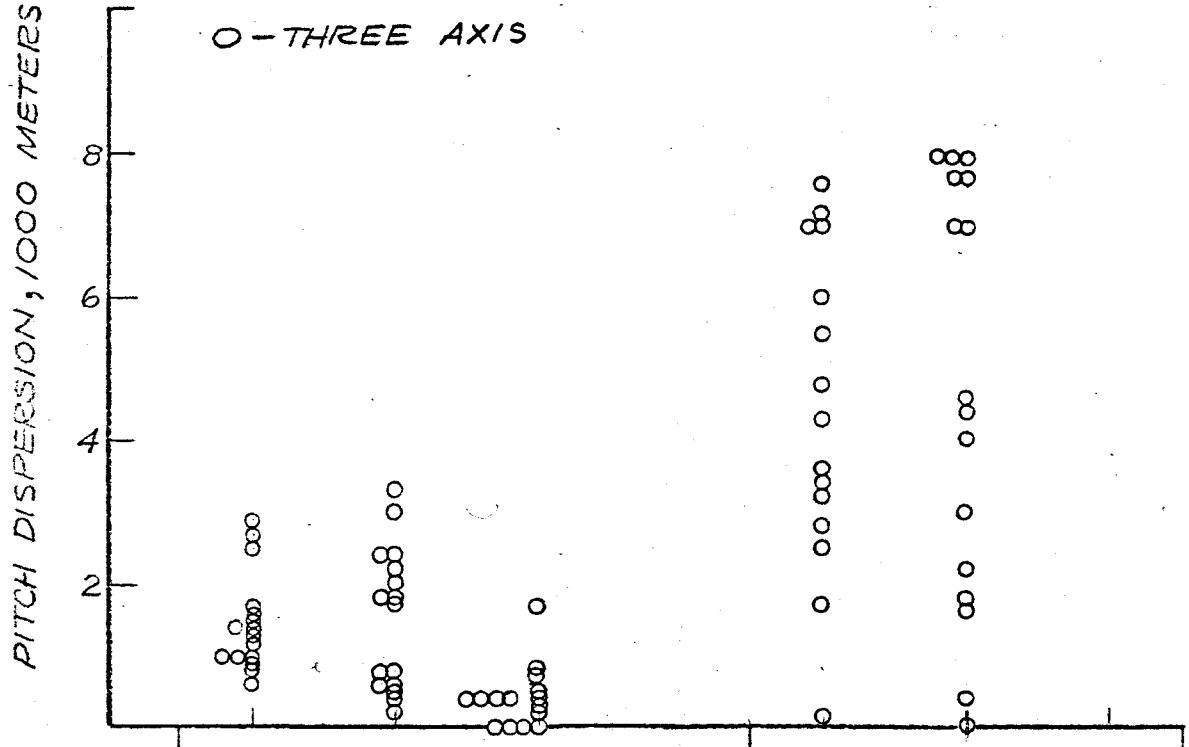

PRIMARY TASK	ATTITUDE STAB.				LOAD CONTROL		
SECONDARY TASK		TRAJ. DISPERSION		RATE			RATE
PRIMARY DISPLAY	$\Delta\phi$	$\Delta\phi$	$\Delta\phi$	$\Delta\phi$	$\Delta\phi, \ddot{\gamma}$	$\phi, x, \ddot{\gamma}$	$\Delta\phi, \ddot{\gamma}$
SECONDARY DISPLAY		$\ddot{\gamma}$	$\ddot{\gamma}, x$	$\ddot{\phi}$			$\ddot{\phi}$

FIGURE 20a TRAJECTORY DISPERSIONS

1) THREE AXIS CONTROLLER
2) DAMPING, $a_1 = 0.75$
3) MAXIMUM CONTROL POWER, 3.5 deg/sec^2
4) CONTROLLER FILTER, $\omega_n = 2.7$ rad/sec
$\zeta = 0.5$

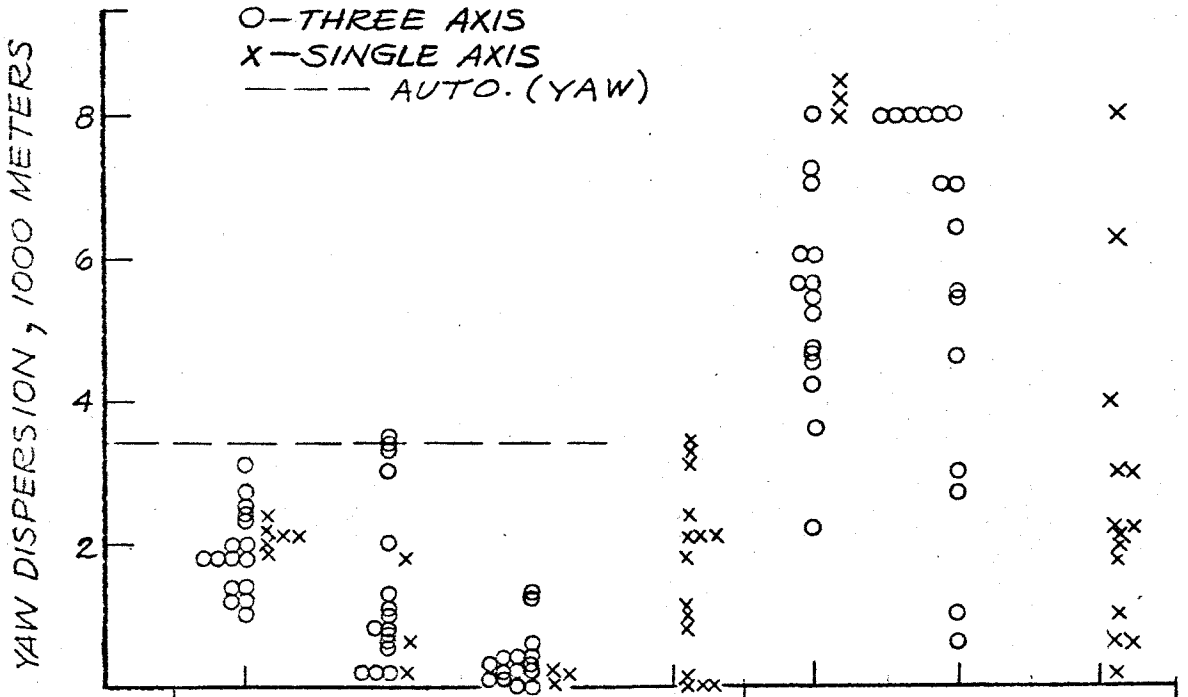

PRIMARY TASK	ATTITUDE STAB.				LOAD CONTROL		
SECONDARY TASK		TRAJ. DISPERSION		RATE			RATE
PRIMARY DISPLAY	$\Delta\phi$	$\Delta\phi$	$\Delta\phi$	$\Delta\phi$	$\Delta\phi, \ddot{r}$	$\phi, x, \ddot{r}$	$\Delta\phi, \ddot{r}$
SECONDARY DISPLAY		$\ddot{r}$	$\ddot{r}, x$	$\ddot{\phi}$			$\ddot{\phi}$

FIGURE 20b TRAJECTORY DISPERSIONS

1) THREE AXIS CONTROLLER
2) DAMPING, $a_1 = 0.75$
3) MAXIMUM CONTROL POWER, 3.5 deg/sec2
4) CONTROLLER FILTER, $\omega_n = 2.7$ rad/sec
$\zeta = 0.5$

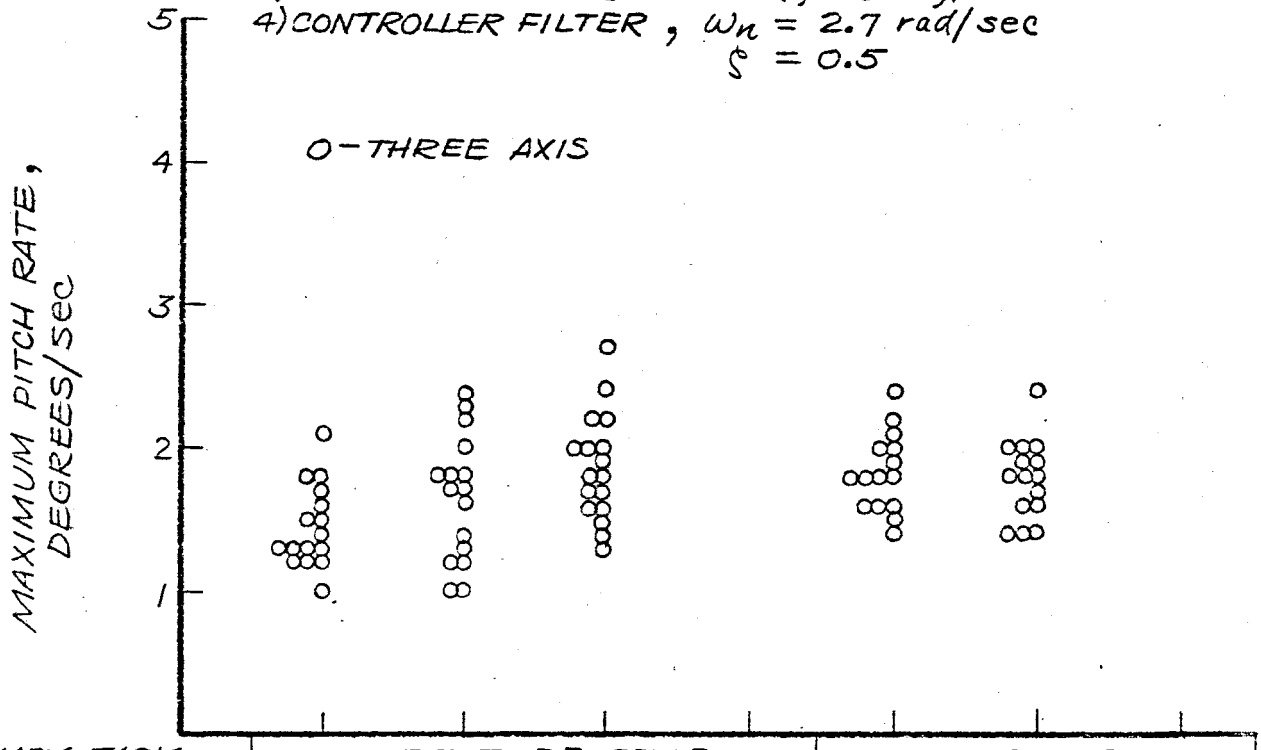

PRIMARY TASK	ATTITUDE STAB.				LOAD CONTROL		
SECONDARY TASK		TRAJ. DISPERSION		RATE			RATE
PRIMARY DISPLAY	$\Delta\phi$	$\Delta\phi$	$\Delta\phi$	$\Delta\phi$	$\Delta\phi, \ddot{r}$	$\phi, x, \ddot{r}$	$\Delta\phi, \ddot{r}$
SECONDARY DISPLAY		$\ddot{r}$	$\ddot{r}, x$	$\ddot{\phi}$			$\ddot{\phi}$
TASK NUMBER	1	2	3	4	5	6	7

FIGURE 21 Q ATTITUDE RATES

1) THREE AXIS CONTROLLER
2) DAMPING, $a_1 = 0.75$
3) MAXIMUM CONTROL POWER, 3.5 deg/sec^2
4) CONTROLLER FILTER, $\omega_n = 2.7$ rad/sec
$\zeta = 0.5$

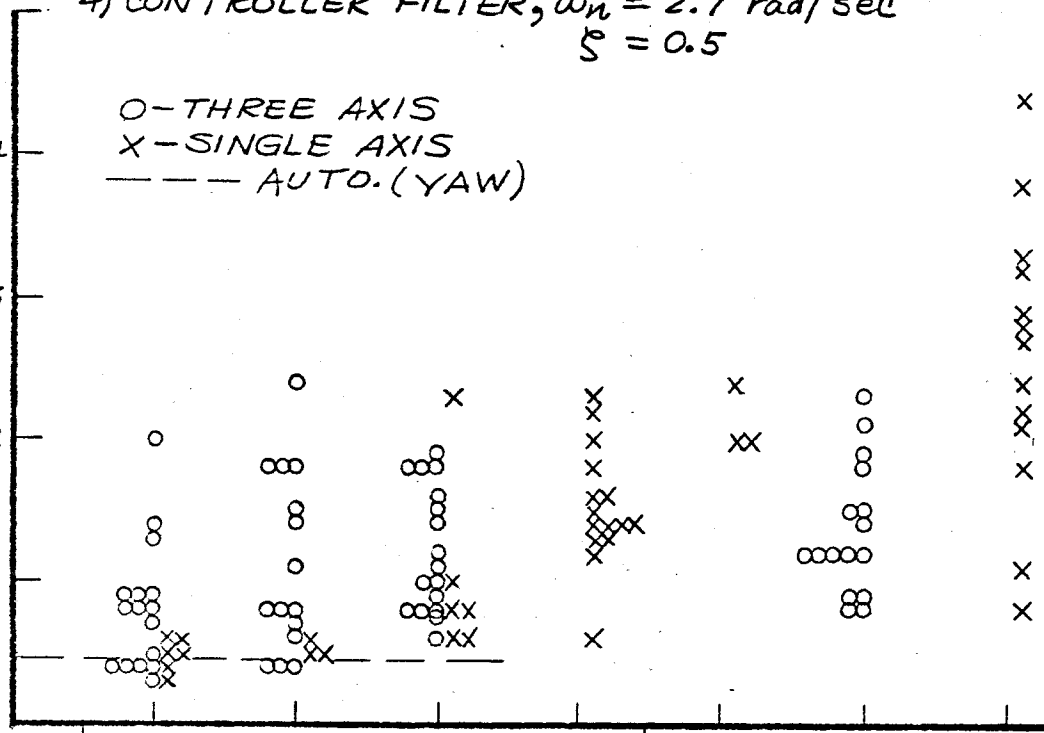

PRIMARY TASK	ATTITUDE STAB.				LOAD CONTROL		
SECONDARY TASK		TRAJ. DISPERSION		RATE			RATE
PRIMARY DISPLAY	$\Delta\phi$	$\Delta\phi$	$\Delta\phi$	$\Delta\phi$	$\Delta\phi, \ddot{r}$	$\phi, x, \ddot{r}$	$\Delta\phi, \ddot{r}$
SECONDARY DISPLAY		$\ddot{r}$	$\ddot{r}, x$	$\ddot{\phi}$			$\ddot{\phi}$
TASK NUMBER	1	2	3	4	5	6	7

FIGURE 216 ATTITUDE RATES

1) THREE AXIS CONTROLLER
2) DAMPING, $a_1 = 0.75$
3) MAXIMUM CONTROL POWER, 3.5 deg/sec^2
4) CONTROLLER FILTER, $\omega_n = 2.7$ rad/sec
$\zeta = 0.5$

O = THREE AXIS

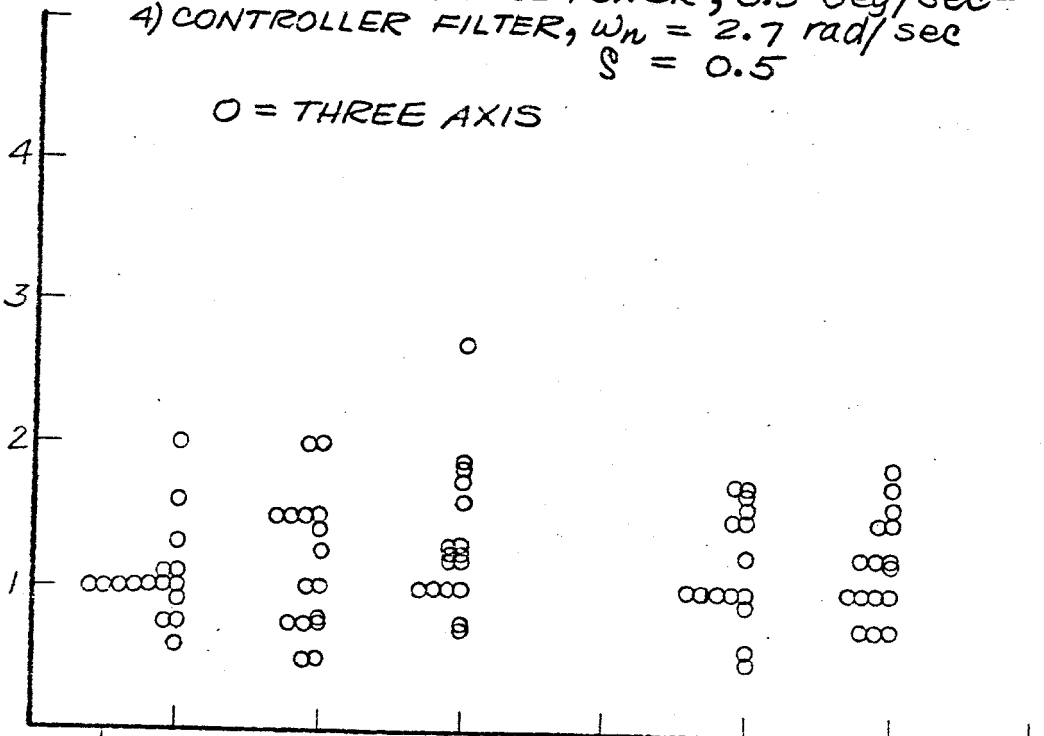

PRIMARY TASK	ATTITUDE STAB.				LOAD CONTROL		
SECONDARY TASK		TRAJ. DISPERSION		RATE			RATE.
PRIMARY DISPLAY	$\Delta\phi$	$\Delta\phi$	$\Delta\phi$	$\Delta\phi$	$\Delta\phi, \ddot{r}$	$\phi, x, \ddot{r}$	$\Delta\phi, \ddot{r}$
SECONDARY DISPLAY		$\ddot{r}$	$\ddot{r}, x$	$\ddot{\phi}$			$\dot{\phi}$
TASK NUMBER	1	2	3	4	5	6	7

FIGURE 22a ENGINE DEFLECTIONS

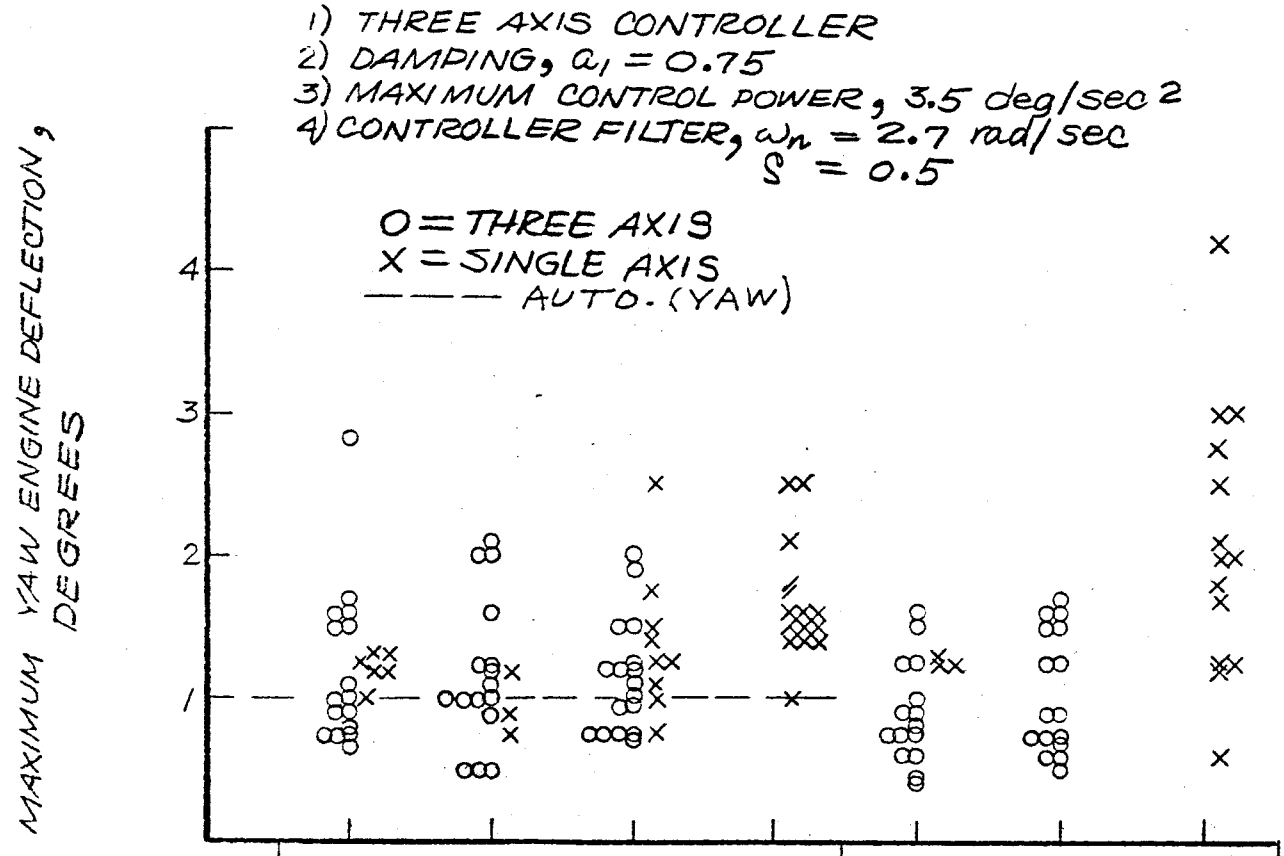

PRIMARY TASK	ATTITUDE STAB.				LOAD CONTROL		
SECONDARY TASK		TRAJ. DISPERSION		RATE			RATE
PRIMARY DISPLAY	$\Delta\phi$	$\Delta\phi$	$\Delta\phi$	$\Delta\phi$	$\Delta\phi, \ddot{\gamma}$	$\phi, x, \ddot{\gamma}$	$\Delta\phi, \ddot{\gamma}$
SECONDARY DISPLAY		$\ddot{\gamma}$	$\ddot{\gamma}, x$	$\dot{\phi}$			$\dot{\phi}$
TASK NUMBER	1	2	3	4	5	6	7

FIGURE 22b ENGINE DEFLECTIONS

1) THREE AXIS CONTROLLER
2) DAMPING, $a_1 = 0.75$
3) MAXIMUM CONTROL POWER, 3.5 deg/sec^2
4) CONTROLLER FILTER, $\omega_n = 2.7$ rad/sec
$\zeta = 0.5$

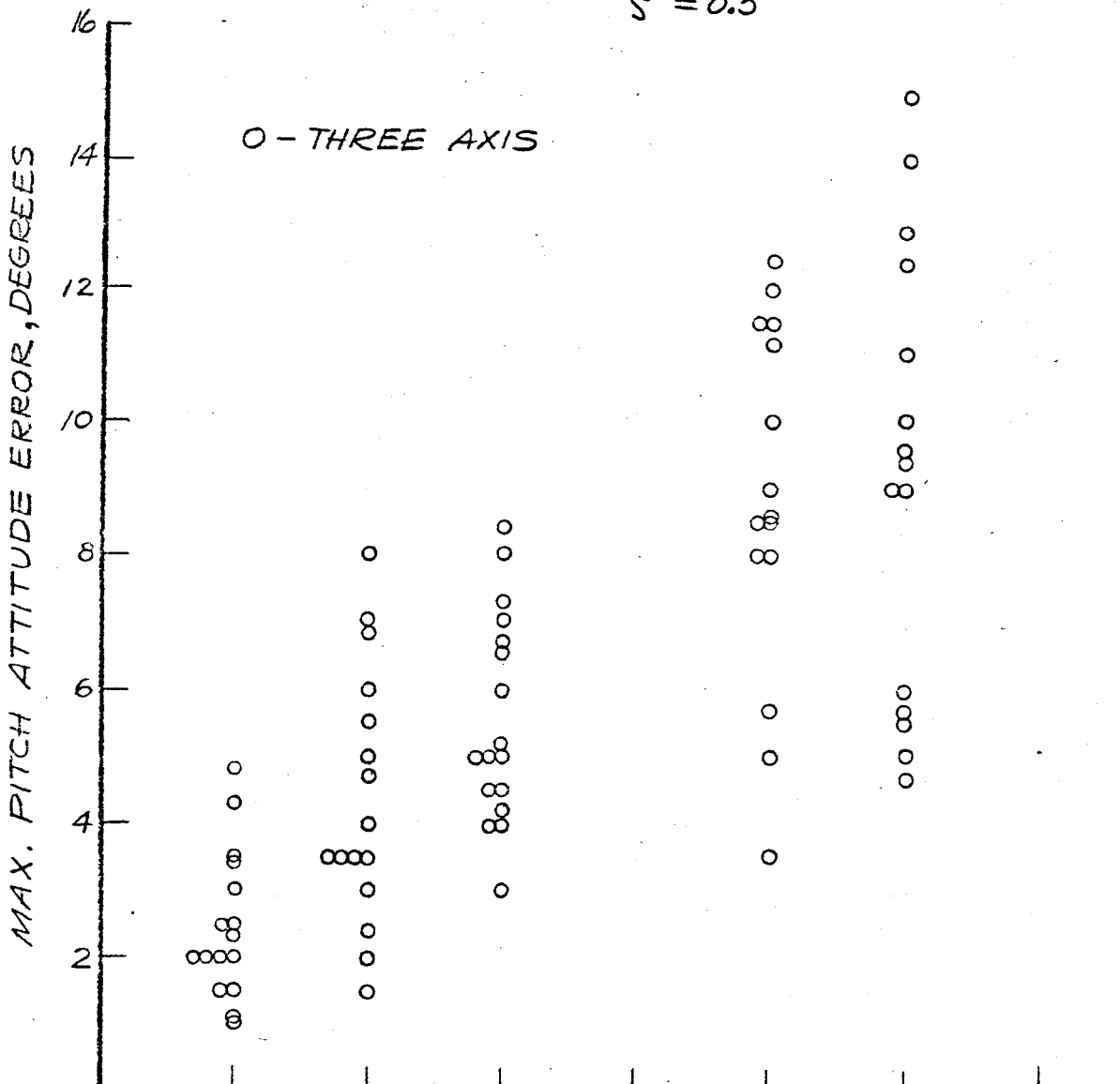

PRIMARY TASK	ATTITUDE STAB.			LOAD CONTROL		
SECONDARY TASK		TRAJ. DISPERSION	RATE			RATE
PRIMARY DISPLAY	$\Delta\phi$	$\Delta\phi$	$\Delta\phi$	$\Delta\phi$	$\Delta\phi, \ddot{\gamma}$	$\phi, x, \ddot{\gamma}$	$\Delta\phi, \ddot{\gamma}$
SECONDARY DISPLAY		$\ddot{\gamma}$	$\ddot{\gamma}, x$	$\dot{\phi}$			$\dot{\phi}$

FIGURE 23a ATTITUDE ERRORS

1) THREE AXIS CONTROLLER
2) DAMPING, $a_1 = 0.75$
3) MAXIMUM CONTROL POWER, 3.5 deg/sec^2
4) CONTROLLER FILTER, $\omega_n = 2.7$ rad/sec
$\zeta = 0.5$

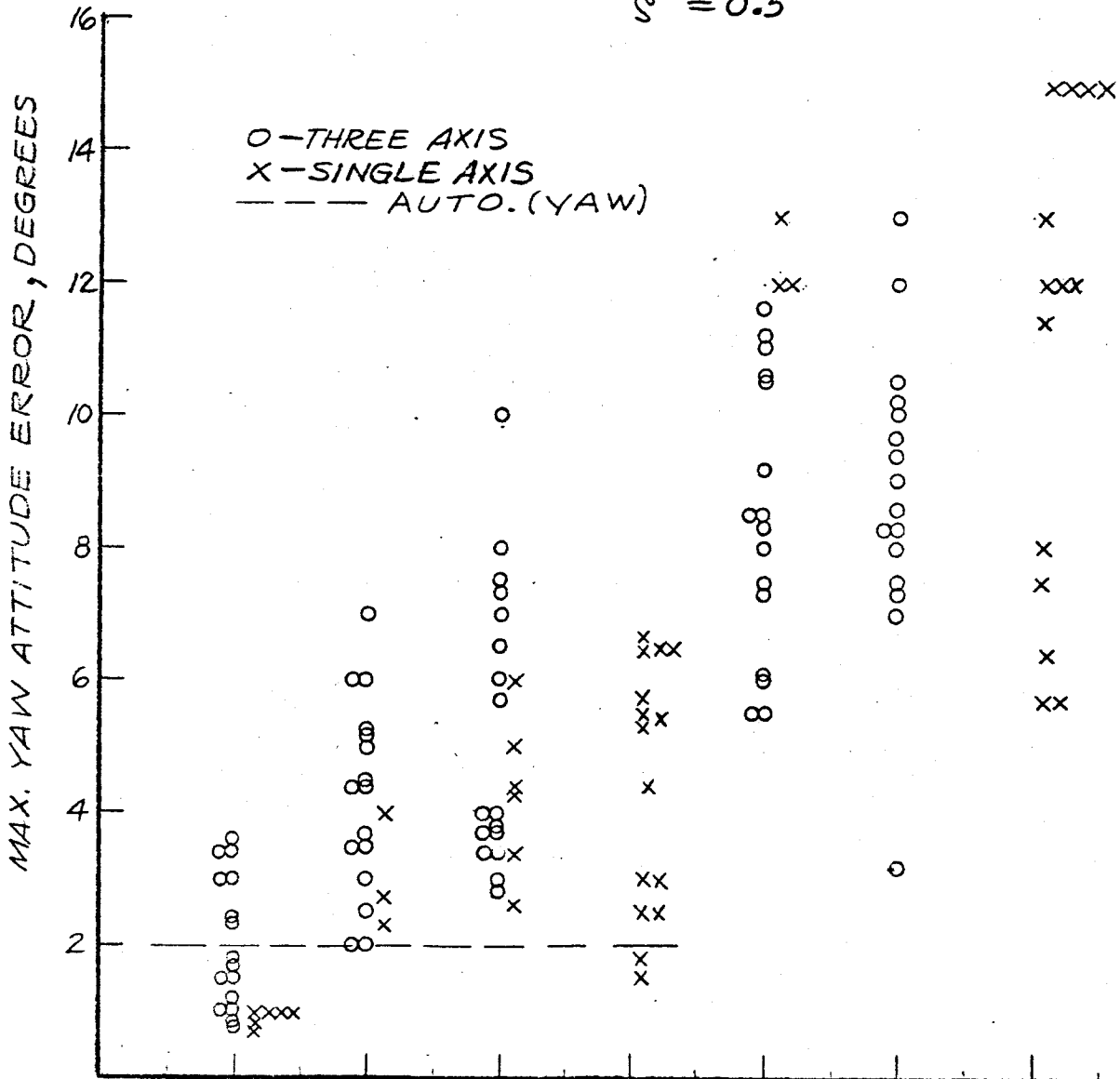

PRIMARY TASK	ATTITUDE STAB.				LOAD CONTROL		
SECONDARY TASK		TRAJ. DISPERSION		RATE			RATE
PRIMARY DISPLAY	$\Delta\phi$	$\Delta\phi$	$\Delta\phi$	$\Delta\phi$	$\Delta\phi, \ddot{r}$	$\phi, x, \ddot{r}$	$\Delta\phi, \ddot{r}$
SECONDARY DISPLAY		$\ddot{r}$	$\ddot{r}, x$	$\dot{\phi}$			ϕ

FIGURE 23b ATTITUDE ERRORS

1) THREE AXIS CONTROLLER
2) DAMPING, $a_1 = 0.75$
3) MAXIMUM CONTROL POWER, 3.5 deg/sec^2
4) CONTROLLER FILTER, $\omega_n = 2.7$ rad/sec
$\zeta = 0.5$

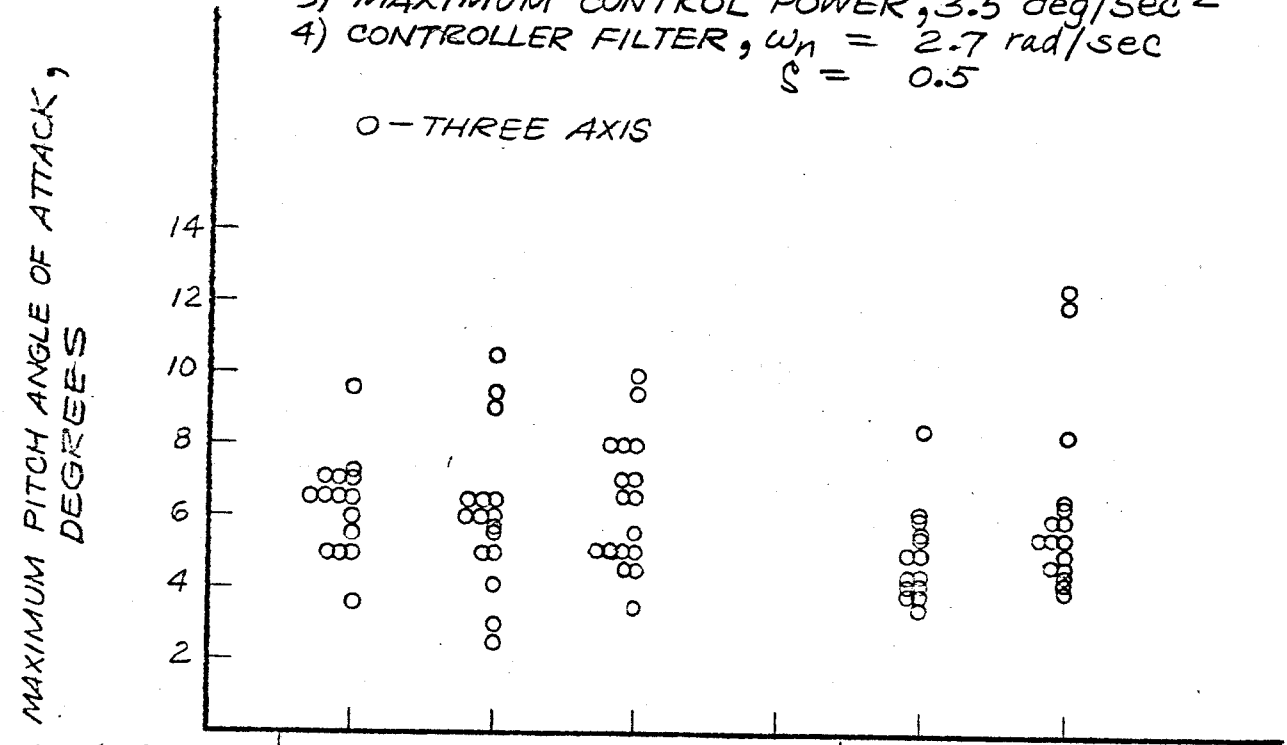

PRIMARY TASK	ATTITUDE STAB.				LOAD CONTROL		
SECONDARY TASK		TRAJ. DISPERSION		RATE			RATE
PRIMARY DISPLAY	$\Delta\phi$	$\Delta\phi$	$\Delta\phi$	$\Delta\phi$	$\Delta\phi, \ddot{\gamma}$	$\phi, X, \ddot{\gamma}$	$\Delta\phi, \ddot{\gamma}$
SECONDARY DISPLAY		$\ddot{\gamma}$	$\ddot{\gamma}, X$	$\dot{\phi}$			$\dot{\phi}$
TASK NUMBER	1	2	3	4	5	6	7

FIGURE 24a ANGLE OF ATTACK

1) THREE AXIS CONTROLLER
2) DAMPING, $a_1 = 0.75$
3) MAXIMUM CONTROL POWER, 3.5 deg/sec^2
4) CONTROLLER FILTER, ω_n = 2.7 rad/sec
ζ = 0.5

O - THREE AXIS
X - SINGLE AXIS
— — — AUTO. (YAW)

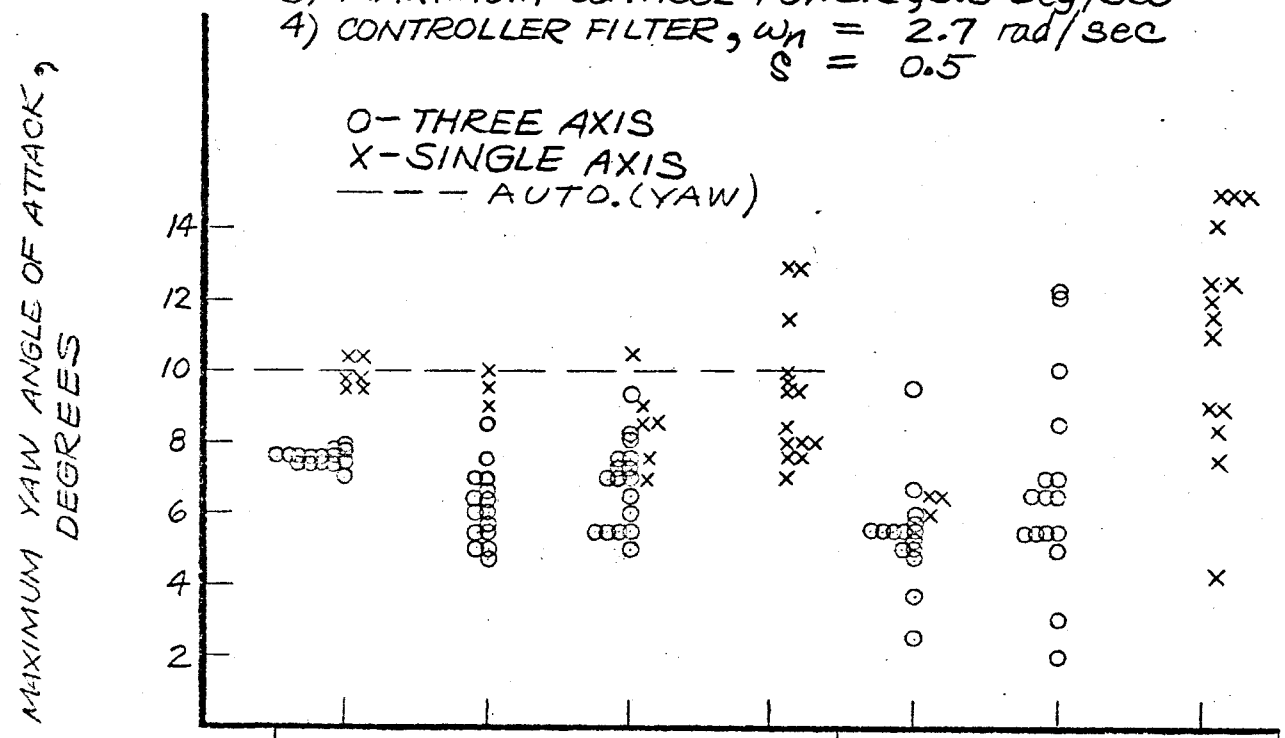

PRIMARY TASK	ATTITUDE STAB.				LOAD CONTROL		
SECONDARY TASK		TRAJ. DISPERSION		RATE			RATE
PRIMARY DISPLAY	$\Delta\phi$	$\Delta\phi$	$\Delta\phi$	$\Delta\phi$	$\Delta\phi, \ddot{r}$	$\phi, X, \ddot{r}$	$\Delta\phi, \ddot{r}$
SECONDARY DISPLAY		$\ddot{r}$	$\ddot{r}, X$	$\dot{\phi}$			$\dot{\phi}$
TASK NUMBER	1	2	3	4	5	6	7

FIGURE 24b ANGLE OF ATTACK